Universität Hamburg
DER FORSCHUNG | DER LEHRE | DER BILDUNG

MASTERTHESIS

Calibrating a Low-cost, 5 Axis 3D Printer

authored by

Tom Schmolzi

MIN-Faculty

Department Informatics

Technical Aspects of Multimodal Systems (TAMS)

Course: Informatics

Matrikelnumber: 7047758

Date of Submission: 01.06.2024

First Supervisor: Prof. Dr. Jianwei Zhang

Second Supervisor: Dr. Florens Wasserfall

Abstract

The field of 3D printing has continuously evolved since the introduction of low-cost machines. One such development are 5 axis machines, which are using 2 additional rotary axes. It has piqued interest in recent times as it promises to deliver better material properties and enable previously challenging processes. Often high quality and expensive components are used to build such machines. Though low-cost approaches like Open5x have been published, the calibration of printers with less accurate kinematic systems proves challenging. In our work we present our low-cost 5 axis 3D printer developed based on the Open5x system and E3D Toolchanger. For this a calibration routine developed for the printer is presented. We were able to achieve stable results by using 3D touch probe attachment in conjunction with algorithms directly run on the 3D printer in GCode. The routine measures the orientation and position of the A and B axes individually by probing the metal axle of the B axis motor and the 3D printed A axis structural elements. Further we show a row of testing patterns which can be printed to check the measured and calibrated values for the rotary axes. Our results allowed us to print a 5 axis movement using a standard $0.4mm$ nozzle with good results. The working repository of this thesis is found under `https://git.mafiasi.de/17schmolz/master_5axis`.

Contents

List of Figures

List of Tables

Listings

1. Introduction

3D printing as a technology has established a firm footing in the industry and hobbyist sectors. It is used ubiquitously for prototyping, small scale productions and specialized applications. The market is further growing strongly, bringing with it many new innovations[35]. Consequently, various techniques have evolved to become used in the low-cost segment like Stereolithography (SLA) printing or laser based sintering printers for metal materials. Based on this, ideas from other related fields are also examined for their feasibility of usage with 3D printers. One such approach is the 5 axis support of popular CNC (computer numerical control) milling machines. Two additional rotational axes are added to the machine to allow it to approach the workpiece from different angles without requiring the operator to intervene and reposition the object. This allows the plastic extruder to directly follow the surface of many complex structures. The UHH (University of Hamburg) has recently built a low-cost, 5 axis 3D printer based on the work by Hong et al. for Open5x [5]. A E3D Toolchanger[38] was used for the printer's frame. Using the frame enabled the usage of varied, purpose-built tools. The structural elements of the kinematic construction of the two rotary axes are mostly 3D printed. In comparison to precise, but also expensive, metal parts, these introduce significant error sources for combined movements. The calibration of the rotational axes is a known problem for CNC mills [8], as the rotational kinematics accentuate small errors based on trigonometric effects. Consequently, our machine proved the need of calibration before usage. The position and orientation of the rotary have to be determined to a high degree of reliability. A calibration procedure is needed. The development of such an approach is the goal of this master thesis. Beyond the considerations of this thesis, complicated 3D deformations of the axes can be present. These can consist of, but are not limited to, bent axes, out of alignment mounting of axes ends or flexing withing the structural elements. Such deformations can cause hard to characterize effects. Further, thermal and other environmental effects were not investigated in this work. However, the considered elements were sufficient to print good results within our tests.

2. Related Work

5 axis 3D printing has been investigated from multiple contexts. Generally the problem of slicing models for 5 axis is one of the most prominent research areas. The calibration of 5 axis systems has been extensively explored in the 5 axis CNC related research. 3D printer specific literature on the topic is sparsely available.

Liu et al. perform a calibration of a low-cost 5-axis 3D printer using a conductive probe and conductive needle-shaped test object [9]. The authors used a line axis model. An error model is used to find the real-world transformation of the axis frames. An accuracy of $\pm$0.424 mm was achieved enabling the usage of a $1.0mm$ nozzle. Our approach and model is inspired by the Liu et al.'s work. Though we required a more automatic measurement procedure, which is not considered by the authors. The usage of a similar or the same error model could prove valuable provided sufficient data collection automatizations.

A model based approach for compensating systematic errors in 5 axis CNC machines is presented by Bohez et al. [2]. For the measurement of the error components reference objects were fabricated. Examination of the tuning pieces enabled conclusions about system. The approach is focused on CNC machines, but could be adapted to compensate for errors in real time on the printer. This is outside the scope of this work.

A 3D probe with a known calibration object is used by Lei et al. to test the accuracy of 5 axis CNC machine's tool and workpiece holder [8]. They construct an error model and use the results to apply error corrections on the fly [7]. The measurements of a sphere on the 5 axis machine inspired the usage of a similar object on the 3D printer. The work uses a custom and high-quality 3D probe not feasible in low-cost scenario.

Hong et al. introduced an accessible 3D printing platform built from commodity parts and 3D printed elements [5]. They further developed a Grasshopper on Rhino based slicer for 5 axis operations. The UHH 3D printer used in this thesis is based on their printer design.

The problem of slicing object designs for 5 axis 3D printing has been investigated by multiple groups. One example is from Ramos et al. where they try to optimize the printing regarding number of supports, surface quality and printing direction [13]. Pawel et al. [11] focus on supportless printing through the use of simulation of the static capabilities of the object. Supports could be avoided when instead the object could be rotated to adjust to the direction of gravity. This is itself constrained by the static load onto elements of the 3D printed object, especially in the rotated orientations.

Shan et al. explore the slicing of objects into non-planar layers on a 2.5D printer and their own 5 axis platform resulting in better surface quality and tensile strength according to their measurements [14]. The authors calibrated the 5 axis platform by executing test prints using the rotary and linear axes independently. The result is examined for alignment issues with manual adjustments made until the system was producing reliable and correct results. Further a high-resolution laser distance sensor was used in their calibration, at the time of writing costing over 3500€.

A modified 5 axis CNC was used by Fang et al. [3]. Their main contribution is in the development of a slicing algorithm for stronger 3D printed parts. The 5 axis printer performs movements specified in object coordinates which are then transformed back into joint space using inverse kinematics.

A slicing algorithm for dissecting 3D objects into multi components printed in different orientations is presented by Xiao et al. [17]. The object is rotated mid-print to then further continue with standard 3D printing for the next section.

5 axis 3D printing enables a multitude of new applications and presents advantages in the physical properties of the resulting objects. The mechanical strength can be increased through control of the printing direction as shown by Luo et al. [10]. The orientation of the layers within the print significantly influence the directional strength of the resulting object.

Electronics is another area of constant development in the 3D printing space. Such approaches could use 5 axis 3D printing to enable more complicated geometry or better integration into already printed objects. The works by Tan et al. [15] and Persad et al. [12] give a good overview of the technologies currently being employed. Hong et al. were able to produce usable electric traces directly extruded on the surface of the workpiece [4]. They found that the usage of a 5 axis machine would improve the quality of the conductive traces compared to layer-by-layer multi-material printing. In future work we would like to use the pressure driven dispenser of our 3D printer to manufacture our own electronics on a 5 axis machine.

3. Research Topic

3.1. Problem Statement

The 5 axis 3D printing platform of the 3D printing lab of the UHH is built from low-cost parts, some of which were 3D printed. We are considering a low-cost printer as such a solution would enable us and other research to work on 5 axis technologies. A 3D printer requires a high accuracy to produce quality parts. Good results have been achieved with standard 3 axis printers even with rather limited calibration measurements of the printer. Though also for such a system the possible variable to optimize are plentiful. Generally the limits of the axes are determined by using end-stop switches. One of the most important factors in the Z height of the nozzle from the print bed. Consequently, print bed leveling is prominent calibration consideration. Often the print bed is probed at many locations to build a topography mesh, which is then compensated for by the printer firmware within the first few layers. In a standard 3D printer the three linear axes can express other errors, like the axes not being rectangular to each other, making the coordinate system non-Cartesian. Bent linear axes can have similar, more chaotic effects. The two added axes of the printer employed at the UHH introduce many new possible spatial configurations and consequently present new challenges in their calibration. The nature of rotational axes pronounce small errors in the base transformation to significant, non-linear positional errors on the surface of a printed object (see figure 3.1). Further 3D deformations of the axes can be an additional source for inaccuracies. The axes can exhibit a wobbling motion, shifting the axis of rotation in some way. The desirable property of the rotational axes being perpendicular to each is likely not given in the real-world.

The additional axes also apply new requirements to the standard, linear axes. The linear axes have to be repeatable in their positional precision, as the location of the rotational axes is an important factor. On a wide print bed the exact location of a printed object is not as important as in our use case.

Frequent changes and repairs of the machine are expected, each requiring a recalibration of the system. A process for accurate calibration of the machine has to be developed to use the machine.

3.2. Project Goal

As a goal for the project we would like to be able to consistently and correctly determine the position of the A and B axes with an accuracy of less than $100\mu m$. Further the measured orientations of the axes should be accurate to below 0.2°. The extrusion width of lines printed onto objects should have a consistent width.

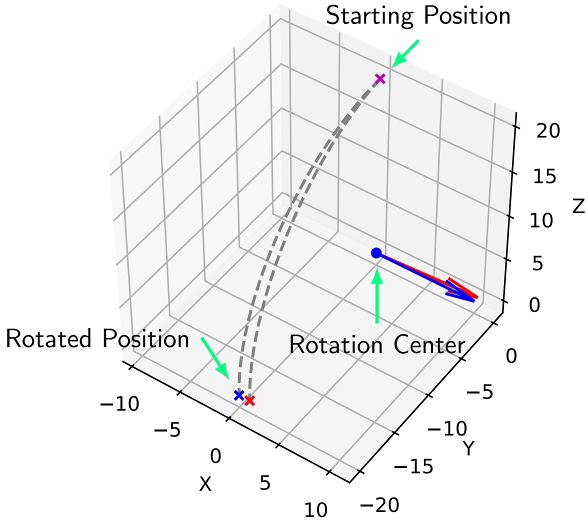

Figure 3.1.: Illustration of the positional errors resulting from angular deviations. The rotational axis is drawn as the blue dot. The idealistic orientation is illustrated in blue. Red marks a $2°$ around Z rotated "actual" axis. The magenta cross is a point on the surface of an object 2 cm from the rotational center. The gray lines show a $90°$ rotation around the axis of the point of the object. The blue cross is the idealistic position, while red is "actual" position. In this example a distance error of $1mm$ on the object is observed.

3.2.1. Requirements Definition

In addition to the general project goal we would like to fulfill the following requirements:

- **Reduce human involvement:** In a current manual calibration procedure a human is involved at every step as no automatic procedure exists. Often adjustments rely on visual judgement of the printer movements. One aim of this work is the reduction of the human in the loop.
- **Time Constraint:** The process used to calibrate the printer in day to day usage should take less than 15-30 minutes as otherwise the usage of the printer needs significant preparation, reducing the productive time of the machine.
- **Financial Constraint:** Often problems with a low-cost printer can be solved by employing high quality measurement systems or replacing parts with more expensive counterparts. In this thesis we want to use low-cost components to make the system accessible to more researchers and hobbyists.

4. System Context

The context of the system consists of the hardware and software utilized in the 5 axis printer system in conjunction with the mathematical model of the kinematics.

4.1. System Model

The printer is implemented as a 3+2 axis system. Meaning three spatial axes along the X, Y and Z direction and two rotational axes, A and B. The A axis is orientated along the X axis, B along the Z axis. The B axis is attached to the A axis. We assume the spatial axes to for a Cartesian coordinate system in the printer. The A and B axes are considered to be approximately aligned with their axes. We model the axes using a point and a vector, describing a line in 3D space. Rotations are then performed around these lines. The position and orientation are described by the three component vectors A_{pos}, A_{dir} and B_{pos}, B_{dir} for each axis respectively.

4.1.1. Machine Origin Definition

The (pseudo-)intersection of the two axes is defined as the origin in the machine with all other axes being relative to that position. To adjust for potential positional offsets in the location intersection we leave the axis limits of the linear axes with 1 cm of buffer room at each end. As the A and B axes are measured in the real world, we cannot expect them to intersect in the mathematical sense. We find the closest approach of both axes and define the point on the B axis as the (pseudo-)intersection (see figure 5.13). The origin is defined once and not moved with 5 axis moves. Consequently, the B axis can move out of the machine origin.

4.1.2. Transformation and Frames

The main operating frame of the printer is one centered on the B axis such that the coordinate $0, 0, 0$ is the point on the B axis closest to the A axis. The A axis is consequently defined relative to the B axis frame. In practice the kinematic chain of the printer ends with the B axis (see section 4.2.4). For this reason the A axis must be transformed from the Z frame and the transformations reversed to get the B axis. The target of the calibration process is to ensure this state using the currently set, uncalibrated frame.

4.2. Hardware

We used a modified E3D Toolchanger [38] as the base printer frame of the project. This allowed for the dynamic usage of up to four different tools in the printer (See Figure 4.1).

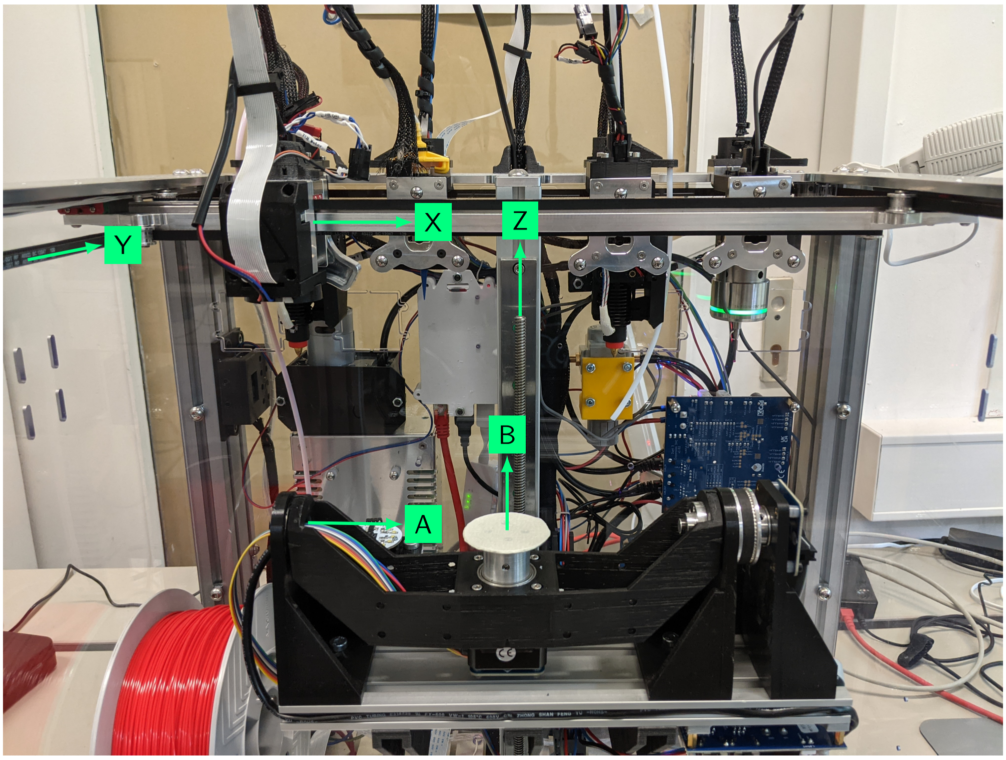

Figure 4.1.: Overview of the 5 axis printer with labeled axes.

The tool-changer's print head is controlled by a CoreXY kinematic chain [41]. An independent platform in the printer is controlled by the Z axis as the print-bed. It has been replaced with our own assembly with two additional rotary axes to facilitate 5 axis movements. Our system is based on Open5x [34] and adjusted for our machine. Additionally, our lab further developed the designs to increase the stability of the parts.

4.2.1. System Overview

An overview of the hardware used in the system is shown in the table 4.1. We only list components deemed relevant for the discussion of the printer.

The printer is controlled by a Duet3D system consisting of the main control board, a secondary expansion boards and two closed loop stepper drivers. The system is interconnected using a CAN bus chain [25]. The closed loop stepper driver boards are used for the A and B axes in their open loop mode. The main board contains all the configuration of the printer and multiple custom GCode scripts for operating and calibrating the printer. It also allows for uploading and running print jobs directly over the integrated web interface, accessed through the included LAN port.

Two Raspberry Pi Camera Modules v2 [40] with controlled LED light rings [21] were added to the printer (see figure 4.8). One camera is attached directly to the toolchanger's print head, giving a top-down perspective. The second camera is mounted to the Z axis bed and

Component	Product
3D Printer Base	E3D Toolchanger
Camera	Raspberry Pi Camera x2
Single Board Computer	Raspberry Pi 4 4 GB x2
Main Board	Duet 3 Main Board 6HC
Expansion Board	Duet 3 Expansion Board 3HC
Closed Loop Driver	Duet 3 Expansion 1HCL
Touch Tool	CNC-STEP 3D-finder
Extruder Drive	Bondtech LGX Lite eXtruder
Hall Sensor	Duet3D Magnetic Encoder

Table 4.1.: Overview of the Hardware used in the 5 axis printer.

points up. The upwards perspective allows for the calibration of the tool's end effector XY position to each other relative to the 3D touch probe. A standard Z probe switch is installed on the toolchanger's head.

Two Raspberry Pi 4 computers [39] are used in the printer. The first main Pi runs a OctoPrint instance for controlling the printer over the serial interface of the main control board. The second Raspberry Pi runs a OctoPrint configured mjpg-streamer[24] instance, which is used to allow the first PI to access the camera feed of the system over the network. One Raspberry Pi camera[40] is connected to each of the computers.

The printer assembly has an internal network using a generic 100MBit switch, connecting the two Raspberry Pi computers with the printer's main board. Using the switch a laptop can be connected to the network for controlling and configuring the system. The main PI additionally is attached to the university network granting it access to the internet. A USB LAN interfaces facilitates the second Ethernet connection of the PI.

4.2.2. Kinematic

The toolchanger print-head is moved through a CoreXY kinematic system [41]. A separate spindle moves the Z axis. The A axis is mounted on the Z axis pointing in the positive X direction. A second axis, the B axis, is mounted to the A axis pointing into positive Z. The B axis would usually be considered the C axis in most 5 axis systems[1]. For our system the C axis was already defined as the toolchanger's stepper motor. According to tests at our lab the CoreXY system moves with an accuracy of $\approx 10\mu m$.

A Axis

The A axis is a rotary axis mounted on the Z axis bed, pointing in the positive X direction. The rotation of the axis is constrained to $\pm 90°$ from the neutral position, with technically up to $\pm 180°$ being physically viable. The constraint aims to prevent unexpected collisions with the A axis for X/Y movements. The greater constraint lies with the cables connecting the B axis motor and hall sensor within the A axis assembly, as they can only be twisted to a certain limit. A stepper motor drives the axis with a 1 to 3 belt drive. A E3D magnetic encoder [26],

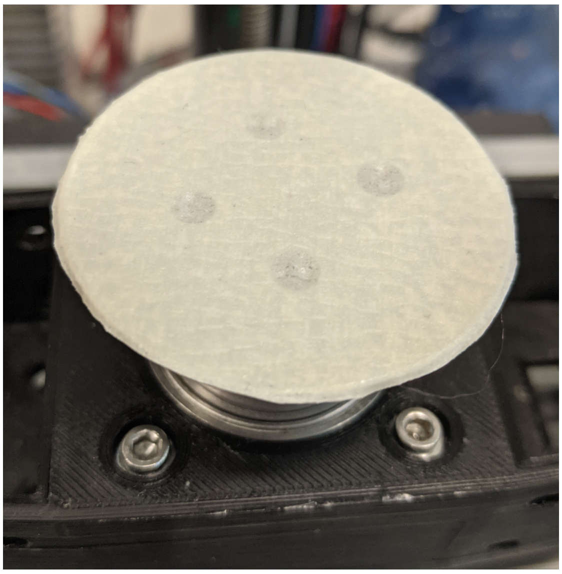

Figure 4.2.: The print bed used in the 5 axis printer attached to the B axis.

a hall sensor, is used to home the axis to a previously calibrated position. The hall sensor is mounted to the A axis assembly. A dipole magnet is glued to the A axis shaft to allow the reading of the axis' position. The measured orientations of the A axis are consequently after the 3 to 1 belt transmission and not directly at the motor. The drive assembly is a potential source of inaccuracies in the movement of the A axis, causing angular errors through the backlash in the belt.

B Axis

The B axis is a rotary axis mounted on the A axis, pointing into the positive Z direction. It directly drives the print bed mounted on it and allows for continuous rotations. A stepper motor powers the B axis without any added drive elements. The axis is homed to a previously chosen position using a E3D magnetic encoder [26]. The encoder is mounted to the bottom of the B axis motor and observes the shaft positions using a glued on magnet. The print bed is mounted to the B axis and allows for the attachment of optional assemblies using tapped holes in the base (see figure 4.2).

4.2.3. Tools

The E3D Toolchanger [38] allows for up to four different tools. The configuration of our 5 axis printer is shown in figure 4.3. Two custom long nozzle, direct drive extruders are installed, allowing for multi-material prints without filament changes. Further a 3D touch probe was installed, enabling the axis calibration of the printer. The fourth tool is either a pick and place module or a conductive silver paste extruder for printing electrical connections.

3D Touch Probe: The 3D touch probe is the tool used for the calibration of the printer

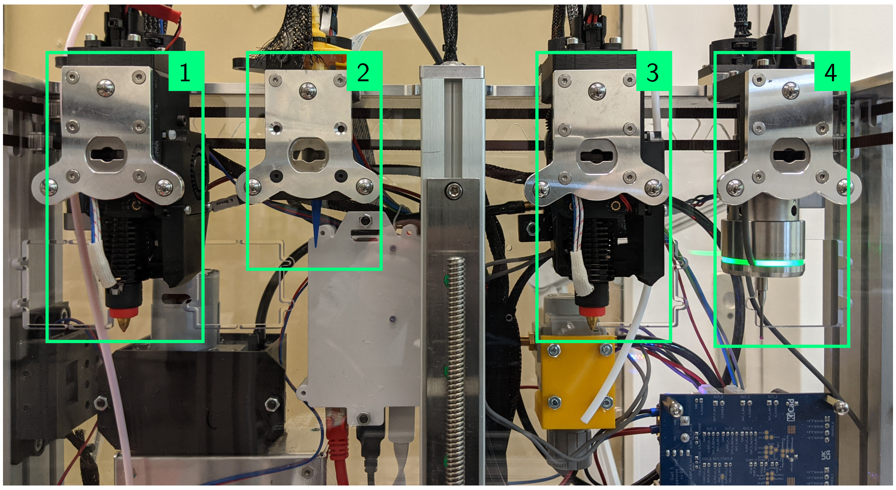

Figure 4.3.: The tools on the printer. From left to right: (1) 2nd extruder, (2) silver paste dispenser, (3) 1st extruder, (4) 3D touch probe

(See figure 4.4). The tool uses the 3D-Finder [37] as its sensor. A small metal rod with a 2 mm ruby sphere at the end is attached to the sensor. It allows for probing objects from both X and Y directions and in the negative Z direction. Within the configuration of the printer the probe is registered as the second Z probe (Z probe number 1). This configuration directly enables probing movements using GCode commands.

Extruder: As our plastic extruders, we use custom long nozzle extruders with lightweight, direct-drive motors. The tools were developed by the technician in our lab using commercially available parts. The hot end is a E3D Revo Belt Nozzle [31] assembly. For the extruder drive a Bondtech LGX Lite eXtruder [18] was used. The extruder is shown in figure 4.5.

Pick and Place: A pick and place tool developed at our lab is also usable with the printer. The usage of pick and place tools with a toolchanger has been explored in previous work from our lab [16]. Using the tool would allow for the placement of electronic components mid-print. The system requires a compressor on the printer to create the vacuum necessary to for the tool. The vacuum is controlled by a solenoid valve.

Conductive Dispenser Tool: A conductive dispenser tool has also been developed at our lab. It is a pressure driven dispenser for silver paste, which creates lines of conductive material. A small compressor is used to create the pressure and an electronic valve controls the dispensing action. As the tool is pressure driven, the paste is extruded at a constant speed. Consequently, for consistent extrusion lines the surface speed withing 5 axis operations has to be kept constant.

4.2.4. URDF

A Unified Robot Description Format (URDF) model of our printer was created as digital representation. We defined a convention for specifying the logical kinematic chain of the printer and connect relevant visuals (See figure 4.6). The visual elements of the printer are

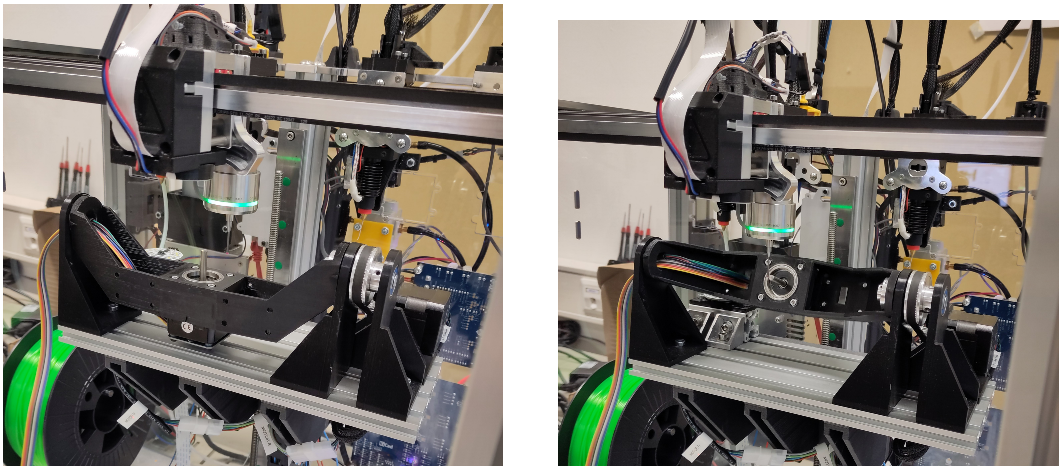

Figure 4.4.: The 3D touch probe's usage in a measurement sequence

based on a combination of our labs design and an assembled E3D printer model found on Thingiverse [32]. The point on the B axis which is closest to the A axis has been defined as the origin of the machine, where $x = y = z = 0$.

The link chain in the URDF begins at the *base_link* and branches off into two directions as shown in figure 4.7. Firstly, the print head chain connects the two links *y_link* and *x_link* with two prismatic joints. Respectively the *y_joint* and then the *x_joint*, matching the real world assembly. Further, end effector frames are attached to the *x_link* with fixed joints. The second chain starts with the prismatic *z_joint*, connecting the *z_link* to the *base_link*. The *a_link* and *b_link* are added with revolute joints, the *a_joint* and *b_joint*.

As the *b_link* frame has been defined to be the same as the *base_link*, offsets and rotations in the previous links in the chain have to be inversely applied. This especially affects the position of the *a_link* joint in the Z plane. An additional fixed joint had to be added to reverse the rotation to correctly apply the offset position between the B and A axes. URDF joints first apply positional offsets and then rotate the frame. To rotate the frame before translating required an extra, rotation only joint.

4.2.5. Electrical Setup

The electrical setup was extended over the laboratory phase of this thesis to introduce new features. Consequently, a few components had to be connected to the printer.

For the Raspberry Pi camera a LISIPAROI LED ring [21] was used to illuminate the tools in the calibration process. The LED ring has four pins, which had to be connected to the printer control system. A IO header on the extension board was used to control and power the lights. Two of the pins provide the ring with 5V power. The power requirements confined the selection of suitable IO headers as by the limits of the Duet3D boards had to be considered. The LED ring is controlled with the last two pins, with one being a common ground connection while the other was connected to the IO out pin.

Duet 3 Magnetic Encoders [26] were used as hall sensors for the A and B axes on the printer.

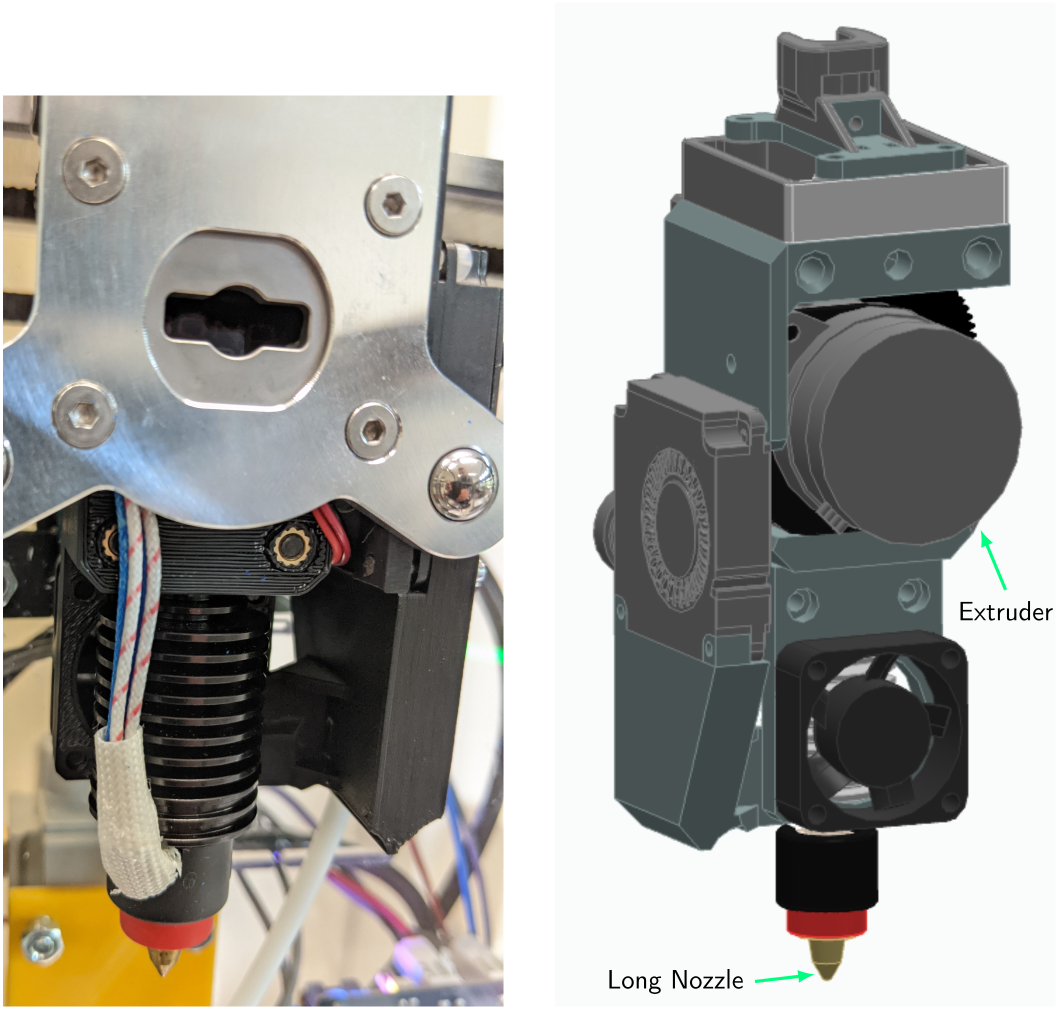

(a) (b)

Figure 4.5.: The custom extruder used in the printer. (a) One view from the back of the real-world assembly. (b) A second rendered front view of the extruder structure is shown.

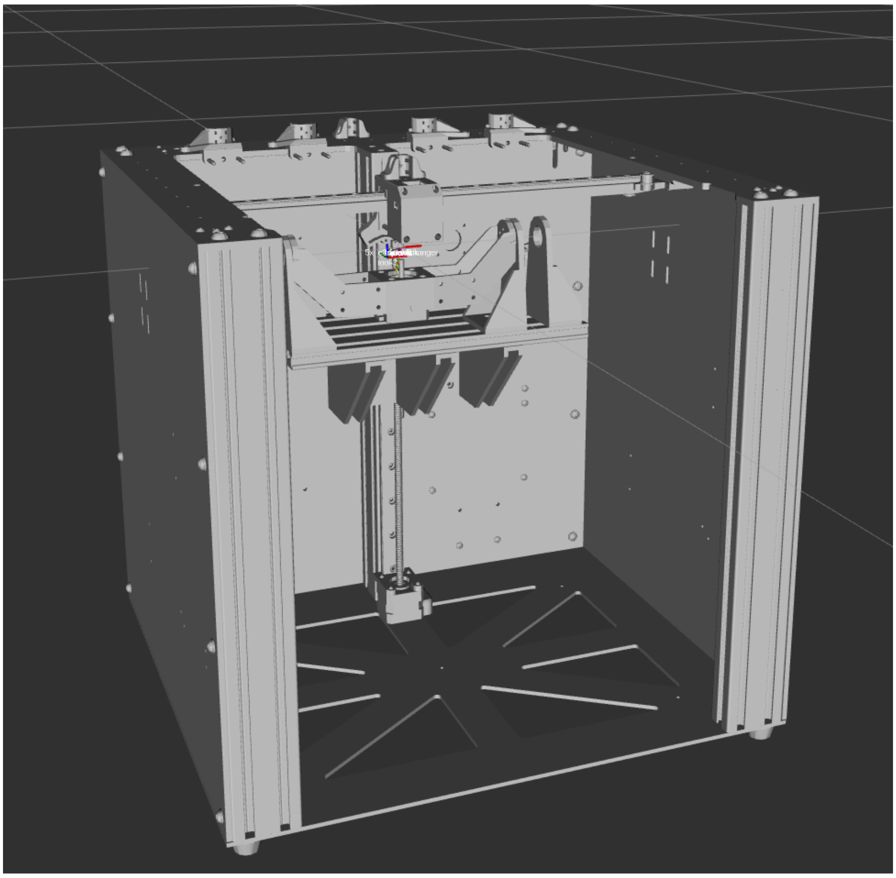

Figure 4.6.: Visual Rendering of the printer's URDF model

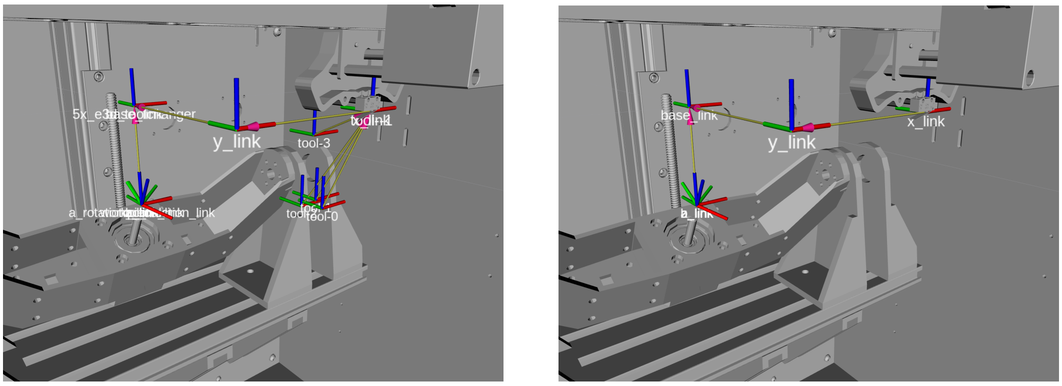

(a) (b)

Figure 4.7.: The printer's URDF frames (a) all included frames (b) reduced frames

The sensors are connected to the closed-loop drivers below the Z bed with a ten conductor ribbon cable. Due to clearance constraints one the of the encoders had their wires directly soldered to the PCB with the plug header removed. The second hall sensor was mounted with an extended length cable.

The 3D touch probe used on the printer was equipped with a four pin miniXLR plug set up for a specific CNC system [37]. Consequently, we built a miniXLR cable which connected the probe directly to the printer. The probe functions between 12 to 24V. A free 12V header was connected to the power leads. The other two leads were direct connections to the electronically controlled normally open switch. We decided to connect the input to ground and the output to one of the input IO headers on the Duet main board. Although not necessary, as 150Ω resistor was connected in series to the switch as required by the manufacturer's documentation to avoid warranty problems. The input pins on the Duet main board are equipped with internal pull-up resistors. The pull-up resistor is used to generate a high signal for open switch position, and a low for the triggered probe. In the firmware the probe is then defined as a digital switch.

4.2.6. 3D printed parts

Most of the 3D printed parts on the printer have been designed, manufactured and assembled by the technician in the lab. In addition to PLA, ABS and carbon-reinforced composites have been used.

Our A axis design was adapted and improved based on the work of Open5x [5]. We adjusted the assembly to fit our Z bed and changed the B motor to directly drive the print bed. Further the stability of the parts has been improved to reduce flex in the system.

The Z axis is connected to the Z spindle by a carbon fiber reinforced, printed connector. An aluminum extrusion forms the main platform on the axis. The A axis is mounted to the extrusion. Further the motor of the A axis and the driver boards for both the A and B axes are attached to the plate. The integration into the control system is enabled by a CAN bus connection. To mount the camera to the Z bed a custom assembly was created. It holds the LED ring and camera while allowing it to connect to a raised aluminum extrusion (See figure 4.8). The holes on the left and right connected to bolts mounting into the V grove of the extrusion. The camera and led ring are held by a combination of plastic pins and M2 nuts inserted mid-print.

4.2.7. Printer Configuration

The printer is configured using GCode files which are run on startup or in certain situations. Most importantly the *config.g* file is run on startup and sets up all the printer functions. At the end of the main configuration, *config-override.g* is loaded, defining the tool and frame offsets. Secondly macros can be created which are GCode files directly usable from the integrated touch display in the form of a button. The Duet3d firmware allows for the specification of frames, which are offsets applied to the axes positional values. Two types of these frames are supported, global printer frames and tool frames.

The global printer frames can be used to set the reference point for all standard movement operations in the printer. We use one of these frames as the B axis based zero point, setting

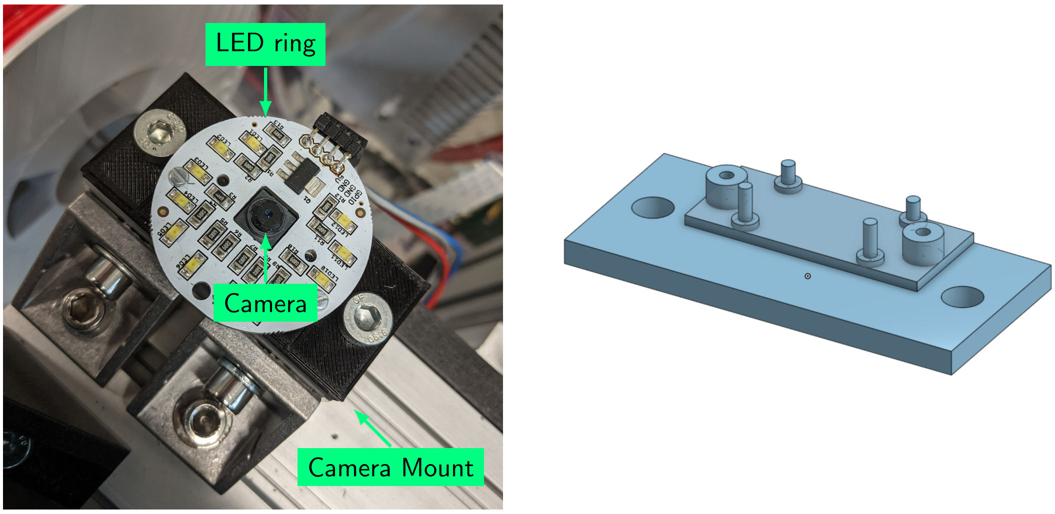

(a) (b)

Figure 4.8.: Bed camera used for tool calibration (a) camera on the print-bed (b) 3D printed camera holding mount 3D model

the calculated point of the B axis as $0, 0, 0$ (see section 4.1.2). General printer functions relying on absolute position, like pick-up operations of tools, can be performed relative to the machine origin frame, ignoring the printer frames. This enables recalibration of the B axis zero point without having to adjust all coordinate based operations run on the printer.

The tool frames are a secondary set of offsets applied whenever a tool is currently actively used. This allows for the adjustment of tools independent of the global printer frames. Given a correct tool calibration different tools can use the same positional commands without extra compensations having to be made. We use this functionality to easily use multiple tools which are all calibrated in reference to the 3D touch probe.

4.3. Software

The software used on or for the printer is described in this section.

4.3.1. GCode Scripts

Most of the needed functionality has been implemented in GCode scripts stored and run directly on the 5 axis printer. The scripts were written in the extended GCode language implemented in the Duet3D firmware. The reference for the standard and extended GCode commands can be found online [27][28]. The extended set allows for the usage of loops, conditionals, calculations, variables and many other lightweight features.

The calibration chain is run by the *Calibration AB* macro (clickable from the screen on the printer). The process consists of four independent scripts (*simple_a_measure*, *sim-*

ple_a_dir_measure, *simple_b_measure*, *simple_b_dir_measure*) and a final script integrating the results to update the calibration (*update_g55*). All the *measure* scripts use the 3D touch probe tool (see section 4.2.3) for their measurements and write their results to the *ab_values.out* file. The *measure* scripts all take X, Y and Z coordinates as a starting position for the routine. The *ab_values.out* specifies the measured elements in a space separated format, where the first entry describes the component and the second the result value. Result vectors are written in the $\{X, Y, Z\}$ format. Singular values are saved as a floating point number. An example output is shown in the listing 4.1.

```
a_axis {0,−0.1650009,−0.2140012}
a_z_in_y 0.0030937
a_axis_dir {0.9994476,0.0332315,−0.0004059}
b_axis {−0.1399994,0.0900002,−10}
b_axis_dir {0.0010010,0.0059996,0.9999815}
```

Listing 4.1: Sample output of one measurement series of the ab_values.out file

Calibration AB: The *Calibration AB* macro is the most important entry point for the calibration chain, as it can be started from the hardware display. The macro calls the different calibration routines after one another, providing the parameters for each. Afterwards the measurement tool is returned to its home position and the frame update executed. The user is prompted to remove the print bed before the start of the calibration process. An optional F parameter can be given with F0 specifying to skip updating the printer frame using *update_g55*, when the macro is run from the console. Additionally, the macro ensures a new, clean *ab_values.out* output file only containing a heading line.

Measurement Scripts: For each of the four main components a measurement script has been developed. The scripts *simple_a_measure*, *simple_a_dir_measure*, *simple_b_measure* and *simple_b_dir_measure* implement the approach described in section 5.4.1. The measured properties are saved into global variables. Additionally, for the *simple_a_measure* the C parameter passes a correction for the 3D probe object size bias in the Y direction for compensation in the A axis Z position calculation (see section 5.4.1).

Frame Update: Using the *update_g55* script, the results of the previous four scripts are combined. The calculation of the closest approach of both lines is preformed by the script. Further corrections for systematic errors are implemented, shifting the X, Y and Z values of the measurements or results as described in section 5.4.2. The script updates the current G55 frame (the B axis $x = y = z = 0$ frame) according to the results. Consequently, it should also only be run once per measurement cycle, as the measured positional values of A and B are relative to the previous frame definition. The resulting offset of the A axis from the B axis is printed to the console. Additionally, the rotation of the A axis in the Z plane is output in radians.

Systematic Analysis

For the analysis of systematic errors in the measurement system, multiple scripts are used. They are either providing convenience functionality or for direct analysis facilities. One script is described in more detail in this section, while more are described in the appendix (see section B).

probe_measure: To repeatably test the trigger behavior of the 3D touch probe (see section 4.2.3) the *probe_measure* script is used. It supports specifying a probing direction vector using the X, Y and Z parameters. The printer then moves into the direction in 0.01 mm steps until the probe is triggered. The movement is reversed until the probe is not triggered anymore. Using the I parameter the amount of times the process is repeated is specified. The feedrate of the movements can be passed with the F parameter. Results of the measurements with the initialization parameters are written to the *probe_measure.out* file. The values are written as space separated rows, where the 3 first elements specify the direction vector and the fourth the feedrate. All following values are measured data-points in the format $\{X, Y, Z, trigger\_value\}$. One row is written per measurement iteration.

4.3.2. Python Notebooks

Jupyter notebooks written in Python are used to analyze results or prototype ideas. Often the data processing and visualization capabilities of Python enabled an easy and fast development of new calibration tools. Further, a few prototypes have been extended to generate GCode test sequences to measure individual properties of the kinematics. Additionally, the analysis of all quantitative test data was performed using the notebooks. An extended list is available in the appendix B.

axes_test: Tests for the components measured for the A and B axes are implemented in the *axes_test*. The tests are simulated, and the results plotted in 3D space. Further GCode compatible with the Duet3D RepRapFirmware for executing the tests can be generated. Only the B position test has been used extensively, while the other three tests are only in prototype state. We used our Rhino based slicer for generating those test cases' GCode operations.

probe_test: Results of the *probe_measure* GCode script (see section 4.3.1) are processed by the *probe_test* notebook. Different analysis are implemented in the notebook. Firstly the hysteresis analysis, for which the data collection had been designed, is processed here (See result at figure 6.2). Further the reliability of the probe in the positive and negative X and Y and negative Z directions is calculated. Lastly dimensional measurement errors of the X and Y probes were tested by comparing measured dimensional results of known size objects.

z_offset: For the determination of the systematic Z bias the *z_offset* notebook is used. Multiple measurements for the Z height of the flat side of the B axis spindle in the $\pm 90°$ A positions are required as inputs to the notebook. Using the known size of the axle as an input the current Z bias of the printer frame can be adjusted (see section 5.1.6).

a_wobble_correct: The *a_wobble_correct* notebook applies a simple post-processing step to GCode files used for 5 axis prints. It implements the correction of the Z value as a movement in the Z coordinate of the A axis has been observed (see section 5.1.8). For each *G1* movement command it first determines the current A axis orientation and then applies an offset based on the correction formula should a Z position be specified. The resulting adjusted GCode is written to a new file.

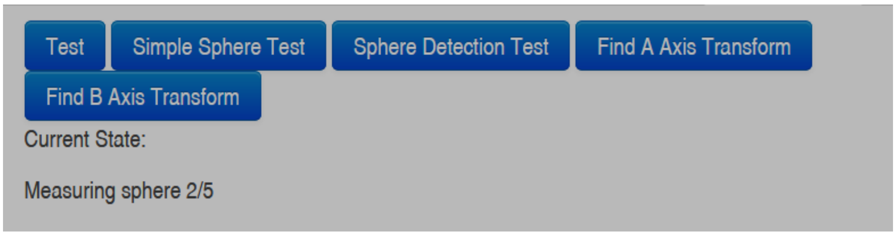

Figure 4.9.: 5x Calibration Plugin Tab with the buttons to enqueue actions and status message below.

4.3.3. OctoPrint Plugin

Two custom OctoPrint plugins were used in the process of experimentation. The newly developed *5x Calibration* plugin and the *OctoPNP* plugin provided through previous works [16].

5x Calibration

The 5x Calibration plugin has been written to allow for the calibration of the printer using more complex algorithms than feasibly implementable in the custom GCode language of the Duet3D firmware. OctoPrint[33] plugins can be written in Python enabling access to many data processing libraries. The plugin implements a custom tab in the OctoPrint interface with simple buttons, which enqueue tasks into a task queue (see figure 4.9). A task generally consists of sending the printer a command and awaiting a message of its results. Tasks implemented the measurement of calibration objects like the sphere or cross (see section 5.2 and 5.3). The task queue is running in parallel to the main OctoPrint process. Further, state updates from the tasks are sent to the frontend and displayed as a simple message.

After the printer has returned results, the task starts processing the data, generally using fitting algorithms prototyped in Jupyter notebooks (See section 4.3.2). Tasks often call multiple operations on the printer, displaying intermediate status messages. The final results are given in a current status message displayed below the buttons on the frontend (see figure 4.9).

OctoPNP

OctoPNP[42] is a plugin previously developed at our lab [16] to facilitate the usage of the pick and place tool head in a 3D printer. One of its functions is the alignment of multiple tools to each other using a bed mounted camera. The functionality has been reused to solve the same problem on the 5 axis machine.

4.3.4. Duet3D Firmware Modifications

The Duet3D firmware [29] of the main board has been slightly modified based on version 3.5.0-rc.3. The closed loop data collection command *M569.5* has been modified to allow for

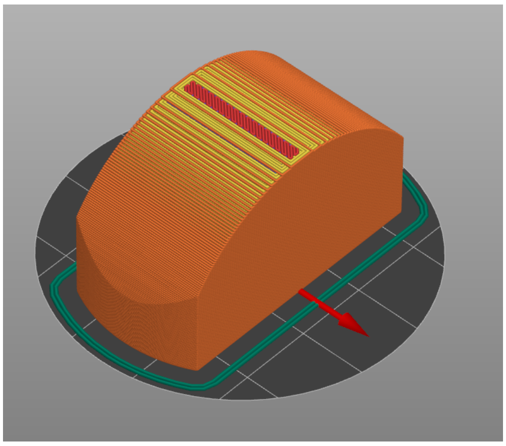

(a)

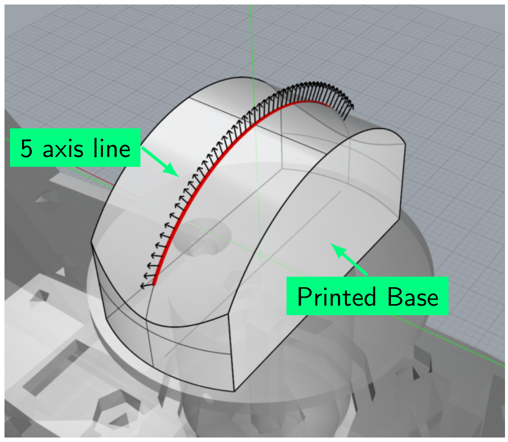

(b)

Figure 4.10.: The A axis orientation test object is processed in both slicers. (a) First the base object is sliced using the PrusaSlicer. (b) Secondly a line on the surface of the object is computed using the 5x slicer. Shown here as a red line.

the processing of raw Magnetic encoder [26] values using GCode, enabling a homing procedure using these values. The extended GCode only supports parsing single line CSV files using the *fileread*. At the point of writing the only way to get the raw step value from the encoder using GCode scripts seems to be using the *M569.5* command, which writes raw values to a CSV file. The modification added is the addition of the optional *H* parameter, to signal stop the command from writing a header to the CSV file, allowing for the usage of *fileread*. Generally a more sophisticated implementation for encoder based homing would be preferred, which is a topic we will start to discuss with the maintainers of the Duet3D firmware outside the scope of this thesis.

4.3.5. Slicer

In a related project a 5 axis slicer has been in continued development. The project is a plugin for the CAD program Rhino 8 [19]. The plugin allows for reading in URDF defined machines models including the A and B axes with their relations. At the time of writing, 5 axis movements for lines on objects can be generated. GCode for the movement can be exported to run the print operation on the printer (see figure 4.10).

The base geometry is sliced using the PrusaSlicer [20] and printed like on any standard 3D printer with a toolchanger.

4.3.6. Additional Software

Python modules like *Matplotlib* or *NumPy* were used to process the results and visualizing them. Further GitHub Copilot in VS Code was used in the editing of the code files using the University provided Pro access to GitHub. Copilot was not used to directly write this thesis.

OpenSCAD was used to create 3D models for the first approaches (see section 5). ROS noetic and specifically the xacro module were used to create the URDF of the printer.

5. Approach

The approach is separated into two main parts, the general calibration of the printer and the measurement of the A and B axes according to the line model (see figure 5.13). Hardware elements of the printer like the tool positions or the characterization of the 3D touch probe are considered in the general calibration section. For the axes determination, three approaches have been tried out. The approaches are listed in chronological order with the last one being used in the active usage of the machine.

For the calibration of the axes and offsets multiple options are available. Generally 3D printers use end-stops for the spatial initialization. Though this helps to find the end positions in the stepper motor space, the axes transformations are expected to be according to the kinematic model of the printer. We consider the current sensors of the UHH 3D printer, especially a Z probe and a gantry-mounted camera. A central idea comes from the world of 5 axis CNC mills, where a tactile probe in conjunction with a known calibration object is used [8]. The probe measures the calibration object on the 5 axis assembly. Through variations in the positioning of the axes systematic errors can be captured in the measurements. Alternative techniques for the measurement of the object exist, like the usage of optical refraction [6]. The data-points on the objects surface can then be used in a mathematical error model of the system. Reducing the error between an idealistic model and actual measurements gives a more accurate model. The fitted model then allows for compensation either on the machine or in the slicing stage. In our work we use a tactile probe and calibration object based approach. The main calibration object is the metal axis of the B stepper motor with the 3D printed A axis assembly also directly being probed. In a second step the correction of the measured error has to be performed. Options for this include changing the kinematic model in the slicer to the actual measured model, baking the changes into the generated GCode. Another option would be compensation on the printer by solving the forward kinematics of the idealistic model as an input to the calibrated models inverse kinematics. We used the slicer based approach by constructing an accurate machine model through the measurements.

5.1. General Calibration

The general calibration discusses topics not directly related to position or orientation of the revolute axes on the printer. The tools and other hardware components are examined.

5.1.1. Tool Calibration

The E3D Toolchanger [38] allows for the usage of multiple tool heads in the printer. The calibration is performed using the 3D touch probe tool (see section 4.2.3) while an extruder

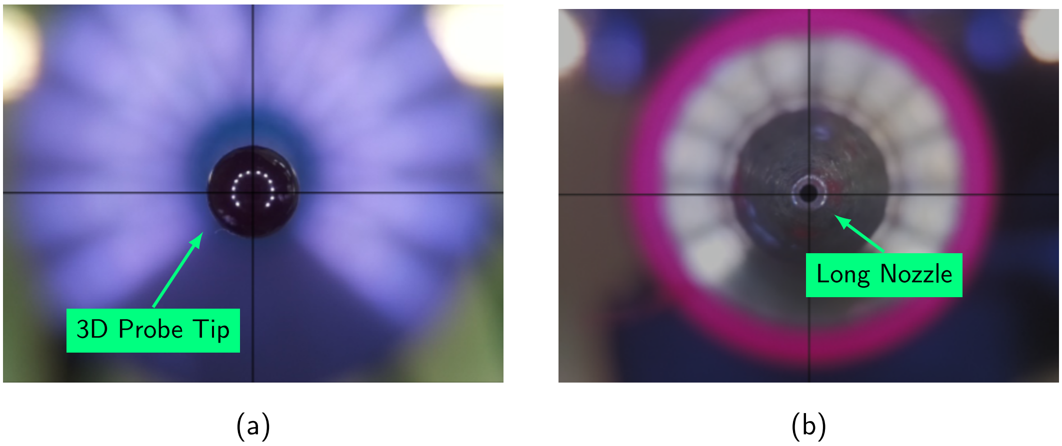

Figure 5.1.: Calibration of the tools to each other. (a) shows the touch probe in the process of calibrating the camera as a reference. (b) the extruder is aligned in the camera image

tool has to be used to do the actual printing. We define the 3D touch probe as the reference tool to which all others are calibrated. The general offset of the 3D touch probe has been set by eye beforehand. For each tool the Z offset is set using the print-bed-paper method [22] using a probed Z height as the reference. The tools X and Y offset to the probe were set using a bed mounted camera and the OctoPNP plugin (see section 4.3.3). The procedure works by moving the touch probe tool into the center view of the bed camera to set the position of it as a reference (see figure 5.1). Then another tool is moved to approximately the same distance to the camera and manually adjusted until the nozzle is in the center of the camera. The plugin then allows for the adjustment of the tool offset such that the nozzle is at the same XY position as the probe tool's end effector. This directly relies on the frames for the tools specified in the firmware (see section 4.2.7).

5.1.2. Printer Homing

The homing of a 5 axis printer requires extra consideration for the rotary axes. For the X, Y and Z axis standard, end-stop based homing procedures are used. The A and B axes are homed using the Duet3d magnetic encoders (hall sensor) [26] (see sections 4.2.2 and 4.2.2). The currently detected step value of the axis is fetched and then a move to adjust to a previously defined target step value is calculated and performed. The target step value for the A axis is defined by moving the A axis against the default Z probe in both directions and defining the middle of the rotation movement as the zero point. For the B axis a position with the flat side of the motor shaft pointing to the negative X direction was chosen by hand.

5.1.3. Pick Up Repeatability

According to the manufacturer of the E3D Toolchanger [38], the kinematic pickup system has a positional repeatability of $< 5\mu m$. Using the 3D probe the combined reliability of the probe and the pickup sequence was tested. The measurement was performed by repeating the sequence of picking up the tool $\rightarrow$ measuring the B axis $\rightarrow$ returning the tool. For the B axis measurements the probe was used in the X, Y and Z direction individually. For Z the top of the axle was probed, X and Y respectively were measured on the flat side of the metal. The flat side was rotated to face into the approximately correct direction. For each loop the orientation is consistent in the bounds of the stepper motor accuracy. The result was then recorded as a three-dimensional vector and statistically analyzed.

5.1.4. Print Bed Measurement

A height map of the metal print bed is recorded using the 3D touch probe. The bed is probed in a snaking grid pattern and the values are written to a CSV file to be processed in the *bed_visualization* notebook. The process is build only for visualizing the print bed and not integrated with a bed mesh compensation on the firmware. In general, it was desirable to confirm the topography of the print bed. The usage of bed mesh compensation for a 5 axis print could be explored, especially for the base objects printed in a standard layered printing configuration. This is not considered within this work.

5.1.5. Touch Probe Tests

In the Touch Probe Test the 3D-Finder tool was used to repeatability characterize the trigger behavior of itself by slowly moving it into the direction of a close-by surface. The motions were performed into of the three spatial axes directions. Then probe was moved back and forth n times in $10\mu m$ steps in of the directions of $\pm X, \pm Y, -Z$. First until triggered and then back until released. The values at each step were recorded and later used to plot the hysteresis of the probe. In a second step the position of the trigger was detected and used for further analysis of the consistency of the trigger point.

By using a known object with a known size the dimensional precision of the measured object could be determined and compared. The reference values were collected using calipers or using the metal shaft of the B axis. The resulting differences x_{bias} and y_{bias} where then used to compensate them in software (see section 5.4.2).

5.1.6. Z Bias

In the calibration the measured Z height of the A axis can be offset up or down. To compensate for this effect a z_{bias} is calculated by probing the B axis spindle in the $\pm 90°$ rotations of the A axis. Z probes to the flat sides of the axle are performed until multiple $z_{90,i}$ and $z_{-90,j}$ have been collected. The Z values should be in reference to the calibrated frame. Using the width between two flat sides of the axle, $d_f = 4mm$, the bias can be calculated as: $z_{bias} = \frac{1}{2}(\overline{z_{90}} + \overline{z_{-90}} - d_f)$ The bias does not consider shifts between the A and B axes as they symmetrically affect the result. The expected A and B axis shift can be computed by:

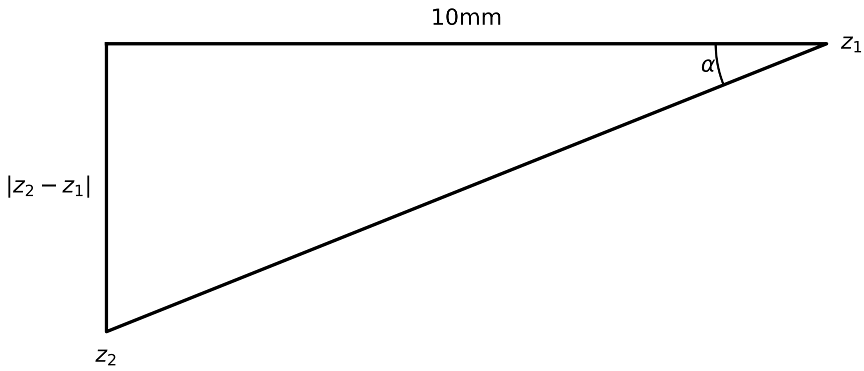

Figure 5.2.: The concept for determining the A axis angular error is shown by plotting the measured Z heights z_1 and z_2 as a triangle lying in the YZ plane. The movement of $10mm$ defines the top of the triangle. α is the angle error of the probed orientation.

$z_{shift} = \frac{1}{2}(\overline{z_{90}} + \overline{z_{-90}})$. This value is used in further calibration procedures (see section 5.1.8). The bias is processed in the machine origin calculation (see section 5.4.2).

5.1.7. A Axis Scaling

In the latter testing phases of the project a problem with the movement of the A axis was detected. Commanded movements did not result in the expected angular change of the A axis. To adjust the A axis, it's angle in the $\pm 90°$ positions was measured. The orientation of the A axis was examined by rotating the B axis shaft such that the flat side could be probed from the top. Two Z heights, z_1, z_2, were collected along the axle with a distance of $10mm$ in the Y direction in each of the orientations. At both ends an error was calculated by defining a triangle based on the measurements (see figure 5.2). The signed angular error is calculated as $\alpha = sin^{-1} \frac{z_2 - z_1}{10mm}$ with the Y coordinate of z_2 being greater than the one of z_1.

To compensate for the error the steps-per-degree value of the axis was adjusted in the printer firmware. This results in a linear compensation of the angle difference along the whole movement of the axis. Present divergences are mostly expected to be a result of the kinematic setup of the system, allowing for gravity to bias the movement of the axis, consequently requiring more steps (see section 4.2.6). A shift of the 0 point could also be found given both orientations show a mirrored offset. After the scaling has been set, the 0 point has to be redetermined (see section 5.1.2).

5.1.8. A Axis Z Shift

In the process of testing the calibration of the machine a divergence between the distance of the A and B axes was apparent when comparing the results of the axes approaches and the Z bias determination. Further, tests confirmed the step-by-step approach correctly found the position of the A and B axes (see sections 5.4.1 and 6.2.1). Consequently, an effect not confirming to the axes model had been found (see section 4.1). The Z position of the A axis expressed a movement observable in the $\pm 90°$ positions while not being present in the $0°$ orientation. A potential explanation for such a movement is the A axis not being perfectly round in its mount and therefore expressing changes based on the influence of gravity. The effect was modeled as a linear Z offset error based on the angle of the A axis. The difference of the distance between A and B from the step-by-step measurements and the Z bias measurement describes this error. The difference z_d has been modeled as being balanced on both sides of $\pm 90°$. Equation 5.1 describes the correction function.

$$z_{wobble} = min\left(max(z_d, -z_d), max\left[min(z_d, -z_d), 2z_d\frac{A}{180}\right]\right) \tag{5.1}$$

The correction was implemented as a post-processing script for the GCode as the used 5 axis slicer does not support the compensation (see section 4.3.2).

5.2. First Approach: Sphere

For the first approach a spherical object was designed to be mounted on the B axis (See figure 5.3). The object has been 3D printed using our ProJet 3510 HD. For the calibration procedure the sphere is then probed using a Z probe in a + shaped pattern. One point is measured at the center intersection and one at each line tip, totaling to five points. The resulting 3D points were then used to find the center of the sphere. First using an analytical solution and later a numeric sphere fitting algorithm [36]. The procedure is repeated for different orientations of the axes, giving a set of sphere centers.

5.2.1. Object Calculation

The five points resulting from the measurements of the sphere are used to find the best fitting sphere without the size having to be specified [36]. Analytic solutions for this also exist and are able to reconstruct a sphere from three points and a known size. Technically two spheres can fit to three points on the surface, but as the measurements are performed from the top, we can assume the lower sphere to be the correct results. To incorporate more than three points, multiple centers can be computed and averaged. Though the fitting algorithm directly addresses this by integrating all 5 points at once, converging to one solution. The algorithm works by encoding the problem as a least squares optimization problem. The center point is found by optimizing for a point that has as close to equal distance to all input points as possible.

5.2.2. Axes Calculation

To get an axis from the measurements of multiple sphere centers, a 2d circle is fitted to the center points. The 3D normal of the circle is the orientation of the axis while the center is the position. A simulated case is shown in figure 5.4, where the input and output are compared.

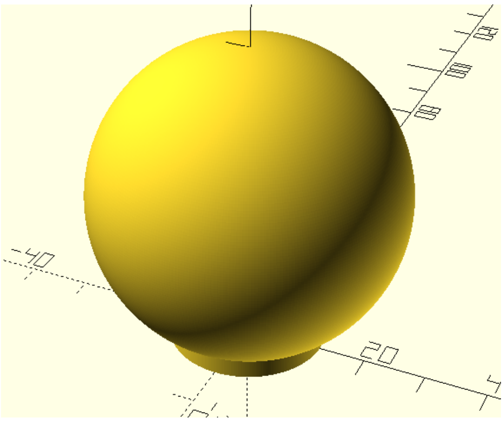

(a)

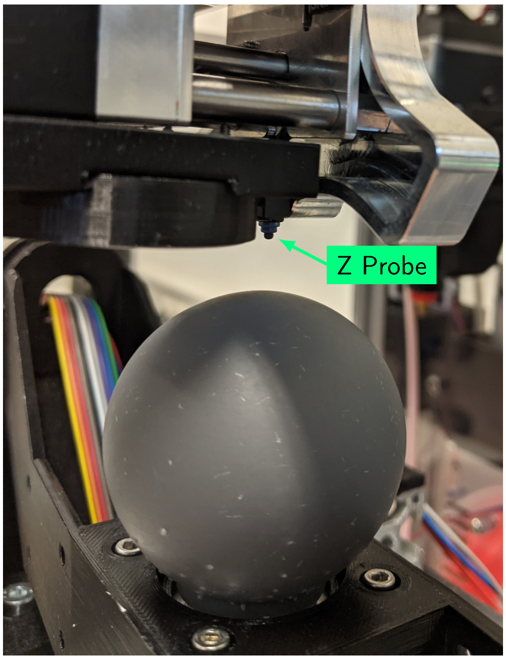

(b)

Figure 5.3.: (a) Calibration sphere for attachment onto the B Axis stepper motor. (b) A real-world image from the sphere measurement.

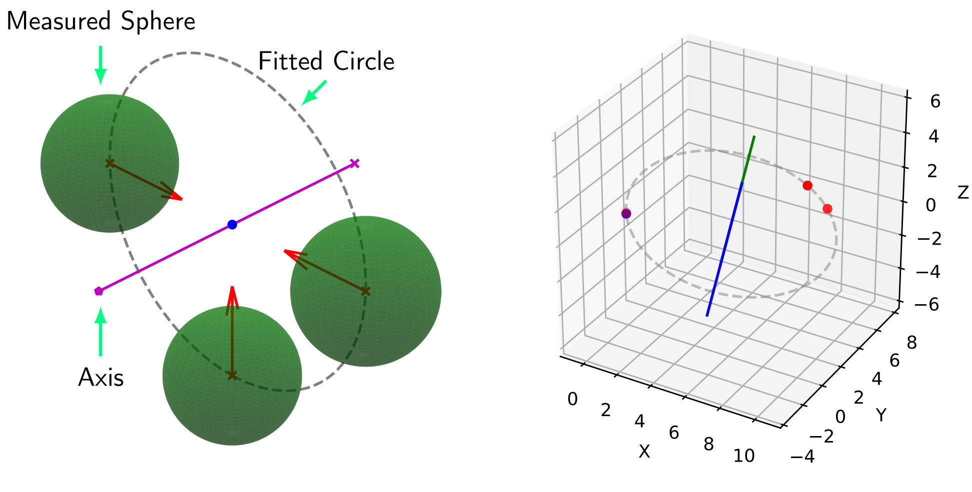

(a) (b)

Figure 5.4.: (a) shows the spheres measured in the different A axis rotations. The red arrow indicates the direction of the upwards B axis. The centers of the spheres are determined, a circle fitted to them and the magenta axis line calculated from the circle. (b) Comparison of a rotation axis fitted to the calculated center points to a simulated input axis. The green line and red points are the input data while the blue line is the result and the blue point (over lapping with a red one) shows a point on the rotation circle.

The fitting to the points assumes the basic line axis model to be correct. The radius of the fitted cycle indicates the mounted offset of the sphere center to the center of rotation. Further effects are hard to observe, as the axis orientation is based directly on the sphere center points. More complex movements of the center, like a shift parallel to the axis would result in an orientation error in the result.

5.3. Second Approach: Cross

For a second approach a calibration cross object was used as a measurement object (See figure 5.5). The cross is more suited to the 3D probe as the surfaces can be mostly aligned with the axes preventing non-linear effects of the touch probe's trigger resistance. The geometry allows for many possible measure series. The terminology *the top of the cross* describes the top of the center structure pointing into positive Z. Further the *arms* describe the structures pointing into the X or Y directions. The *arm size* is the width of the arms and *arm length* the distance from the center structure to the ends of the arms.

The main approach developed was a three-phase measurement process of the cross. The process is able to process B axis rotations of $45°$ intervals or A axis rotations of $-90°, 0°, 90°$. For the B axis these have been chosen by design and could easily be extended to any rotational value. The limitations for the A axis result from the geometry of the cross itself. The measurement algorithm expects to be able to probe the plane on the arms from the top. A requirement for reliable probing results are roughly flat surfaces which approximately lie in the Z plane. For other A axis angles major changes in the measurement procedure would have to be implemented. Only one axis can be rotated at once with the other being set to $0°$.

The measured points of the phase are visualized in the figure 5.6.

First phase: The measurements of the first phase are visualized in red. Firstly the top of the cross is probed to check the Z height of the object. Then the sides of the top are probed from the side at a Z value 5 mm below the probed top. The measurements of this phase are mostly used as the basis of the later phases and not in the process of finding the cross pose.

Second phase: For the second phase, the side arms of the cross are probed from the top. The visualization shows these points in magenta. The basis of the probed points are the measured side positions from the first phase. The results of these probes are used to find the orientation plane of the cross, spanning the top surfaces of the arms.

Third phase: In the third phase the sides of the cross arms are measured. The points are shown in blue. The previously measured top points on the cross arms are used as the base positions for the side probes. The probes are made left and right of the results at the approximate center Z height of the arms. The side measurements are used to determine the center point of the cross object. The resulting center point and cross orientations are then used to calculate the axes orientations and positions.

5.3.1. Object Calculation

The resulting 3D points from the measurements were then used to determine the orientation and position of the calibration cross (see figure 5.6).

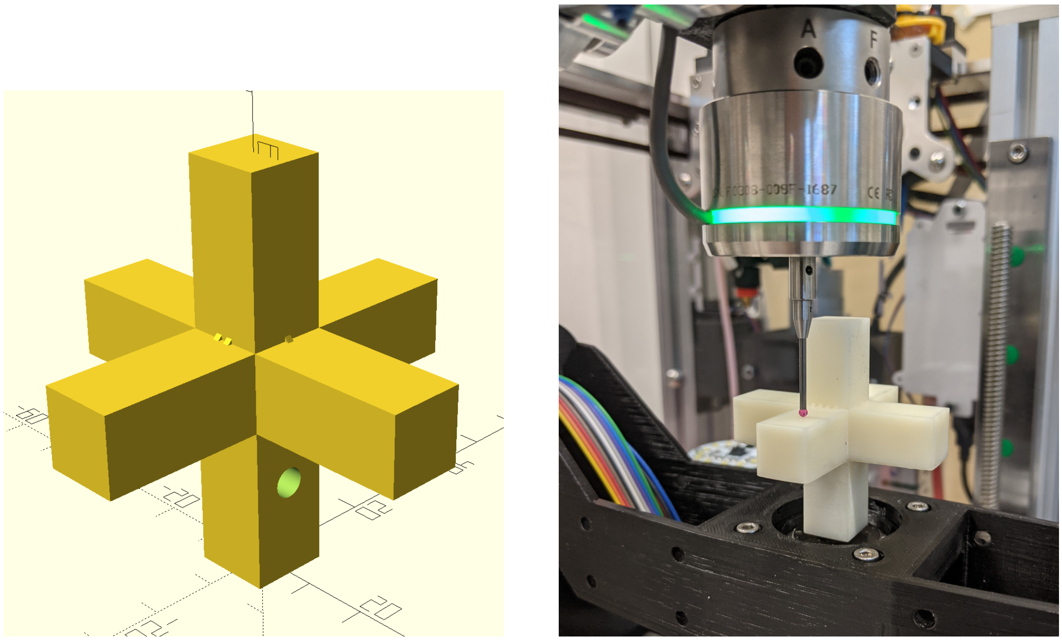

(a) (b)

Figure 5.5.: (a) Calibration cross for attachment onto the B Axis stepper motor. (b) shows a measurement of the one of the second phase's points.

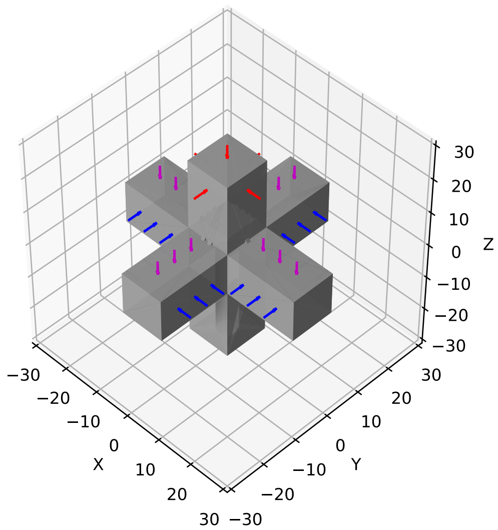

(a)

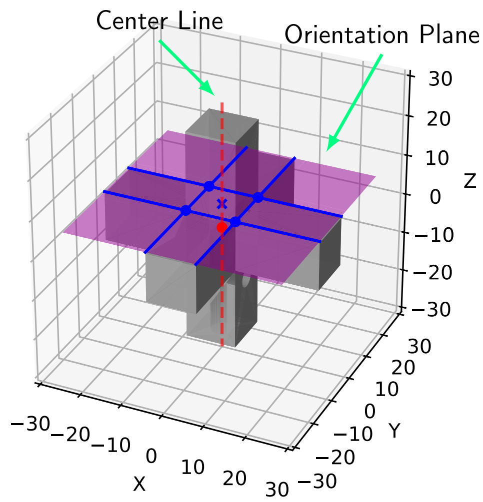

(b)

Figure 5.6.: (a) Measurements point vectors on the calibration cross, separated into phase by color. The first phase is marked in red, the second in magenta and the third in blue. (b) The fitted properties of the cross are shown in the same colors as the data collection. The magenta plane is fitted to the magenta points. The blue points are projected into the plane and lines fitted to them. The intersections of the lines near the center are found. The blue x marks the center of the intersections, which is on the dashed red center line. In the last step the actual center, marked by a red dot, is calculated.

The data of the phases is collected in separate lists. First a plane is fitted through the points collected on top of the cross object's arms using Singular Value Decomposition (SVD). The third component describes the normal of the plane, while the mean of all points is a point on the plane. Using these two properties, the plane can be determined. The normal of the plane is the orientation of the object in the Z direction.

To get the position of the center of the object, first the center line in Z of the object is found. For this the measurements of the sides of the arms are projected into the 2d orientation plane. The points were separated into left and right of each arm for each axis (resulting in four groups). To each of these groups a line is fitted in the 2d space. The four intersections of these lines close to the center of the object are calculated. Intersections between the approximately parallel lines are skipped.

The intersections of these lines are expected to lie on the corners of the center, Z structure when viewed from the top. As such the average of the intersections gives a point which should define the centerline of the cross in the Z direction on the arm top plane.

The point is transformed back into 3D space and together with the orientation normal gives the center line. To calculate the center point the point is moved in the negative Z direction by half of the arm size of the cross. This moves it down from the top of the arms to the center height. Other than for this operation the size of the cross is not used in the fitting process.

For the cases of the A axis being rotated, the object orientation has to be rotated as well, as the measurements are always performed in the negative Z direction. The normal of the cross will always point up, even in the rotated measurement cases, where the cross is actually pointing to the side. Using the two projected lines in the X direction in the 2d projected space, an X direction orientation of the object is found. The lines lie along the arms of the cross in the X dimension. The orientation of the lines is combined and shifted back into 3D space. The cross normal is then rotated around the X orientation vector to compensate for the A axis rotation in the object frame without requiring exact knowledge of the A axis orientation. The rotations are performed within the cross structure to select the correct arm pointing to the side. As such the orientation and position of the calibration cross is resolved. Optionally the rotation around the orientation vector could be found to fully define the 3D pose of the cross. By always using the measurements from positive and negative directions for each of X and Y axes, systematic errors regarding the dimensional accuracy of measured objects are expected to cancel out. Based on later performed measurements, this assumption proved partially wrong as directional biases were found (see section 5.1.5).

5.3.2. Axes Calculation

The axes are measured by repeating the measurements in different configurations of the axes' rotations. For both the A and B axis a 2d circle is fitted through the centers of the measured crosses. The center of the circle gives a point on the specified axis. The average distance of the points to the center point gives an off-axis center mounting position of the cross. A combined value of the shift from the mount and the axis can be determined. Secondly the orientations of the cross objects are used. A 2d circle is also fitted in the vector space of the orientations with them being interpreted as 3D coordinates. The orientation of the circle then gives the orientation of the rotated axis. Further the rotation of the mount and the average

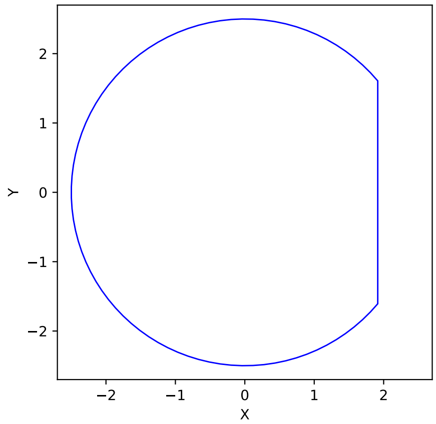

Figure 5.7.: Top view of the B axle geometry

rotation of the object is found, by inverting all rotations around the axis and averaging the resulting orientation. The cross approach allows for the measurement of more properties than the sphere approach given the structure of the object. Some parameters beyond the line model could be determined using the cross method, as the orientation of the axis is determined by the object normals. As the 2d circle is fitted in an already predetermined plane, systematic variations in the center point positions could be separated. Often the mounting of the B axis would also influence these points, though in a rotation-symmetric way. More complex 3D deformations could be distinct separated in the measurements, provided the noise in the values is sufficiently low.

5.4. Third Approach: Step-by-Step

The approach described is based on measuring the axes using the metal spindle of the B axis stepper motor. A view of the profile of the axle is show from the top in figure 5.7. Using the B axis stepper motor to rotate the axis a pseudo square prism can be constructed as a measurement object. A demonstration of the measurement approach can be viewed under `https://youtu.be/AuEFCgAx3H4`.

5.4.1. Components

The calibration of the A and B axes is separated into four components. The position and orientation for each axis. Each measurement can be performed independent of the others and all use the 3D touch probe (see section 4.2.3).

A Position

The process for determining the A axis position uses three measurements and one additional calibration parameter, c_y (see section 6.1.1). Firstly in the $A = 0°$ position the Z height (z_0)

of the B axis spindle is probed. Secondly the Y position of the top of the spindle is measured in the $A \in \{90°, -90°\}$ rotations as y_{90}, y_{-90}. For all probes the x position is commanded as 0.

The values are then combined to describe a circle in the YZ-plane (visualized in figure 5.9). As the orientation of the A axis is unlikely to directly lie on the X axis, the method includes an inherent error source, though only a small deviation is expected. The case for a radius of $5mm$ and $5°$ of rotation around Z results in $19\mu m$ of error in the Y component of the position (see equation 5.2).

$$E_y = 5mm - \frac{cos(5°) - cos(185°)}{2} \cdot 5mm \approx 19\mu m \tag{5.2}$$

The small circles represent the $2mm$ ruby sphere at the tip of the 3D probe. As such $r_p = 1$. The resulting A position is described in the equation 5.3. A_{pos} is relative to the center of the XY position and the bottom Z of the 3D probe's tip.

$$A_{pos} = \left[0,\ \frac{y_{90} + y_{-90}}{2},\ z_0 + \frac{y_m - c_y}{2} + r_p\right];\ y_m = |y_{90} - y_{-90}| \tag{5.3}$$

A Orientation

For determining the orientation of the A axis a part of the 3D printed axis structure is probed, which has a shape comparable to that of a cube. The orientation is determined by calculating the slope in the measured values in multiple dimensions (see figure 5.10). First four Z values are collected as a Z direction probe from the top surface ($z_{x,1}, z_{x,2}, z_{y,1}, z_{y,2}$). Further four points are probed in the positive and negative Y direction at two different X heights, giving two groups. The slope of Y and Z in the X direction are calculated according to the equation 5.4 (m_{yx}, m_{zx}). The direction of the A axis is then given by normalizing the vector in the positive X direction and the two slope values. Additionally, m_{zy} is calculated, which indicates how level the A axis is. The value is used to check the homing of the A axis. Though the actually probed slope is the top of the A axis and not the actual B axis orientation.

$$\begin{aligned}
m_{zx} &= \frac{z_{x,1} - z_{x,2}}{2d_{zx}} \\
m_{zy} &= \frac{z_{y,1} - z_{y,2}}{2d_{zy}} \\
m_{yx} &= \frac{1}{d_{yx}} \cdot \left(\frac{y_{x1,2} - y_{x1,1}}{2} - \frac{y_{x2,2} - y_{x2,1}}{2}\right) \\
A_{dir} &= normalize\left([1, m_{yx}, m_{zx}]\right)
\end{aligned} \tag{5.4}$$

B Position

The position of the B axis is found by probing the B axis spindle from the negative and positive X and Y direction (see figure 5.11). For probes in the X direction, the Y component is kept constant. Similarly, for Y probes X is a commanded value. The Z height is set as

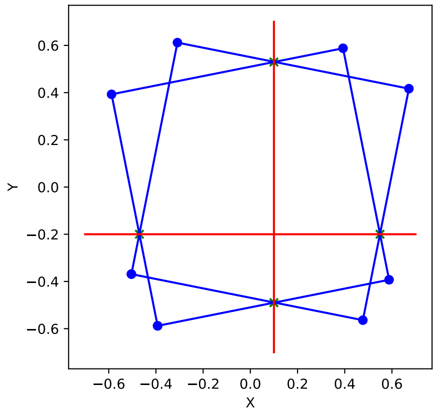

Figure 5.8.: Evaluated option for the third approach using the flat side of the B axis shaft as a square by rotating it for 90° between measurements

$Z = -10$. For the position of the B axis the two measurements of X and Y, x_{p_1}, x_{p_2} and y_{p_1}, y_{p_2} are averaged individually for the matching probes. The two averages define the center X/Y coordinate of the axle. B_{pos} is relative to the center of the XY position and the bottom Z of the 3D probe's tip.

$$B_{pos} = \left[\frac{x_{p_1} + x_{p_2}}{2}, \ \frac{y_{p_1} + y_{p_2}}{2}, \ -10 \right] \tag{5.5}$$

The square prism based approach cannot be used to find the position of the B axis as four points on the surface of a square often have more than one solution fitting the data (see figure 5.8). Though the better the alignment of the square to the axes is, the closer the two possible centers would be. Multiple measurements per side of the square are limited to a small 1 mm distance, introducing high noise potential. The square prism proved more useful for determining the orientation of the axle.

B Orientation

For the measurement of the orientation of the B axis the flat side of the B axle is probed at two heights from $\pm X$ and $\pm Y$ ($z_{1,2} \in \{-10, -15\}$). To facilitate this, the flat side is always rotated into to probing direction, effectively creating a square prism (see figure 5.12). The four measurements at each height are then averaged and the vector between the points gives the direction of the B axis as described in equation 5.6.

$$\begin{aligned} p_1 &= \frac{1}{4}\sum^{i} p_{z_1,i} \\ p_2 &= \frac{1}{4}\sum^{i} p_{z_2,i} \\ B_{dir} &= normalize(p_2 - p_1) \end{aligned} \tag{5.6}$$

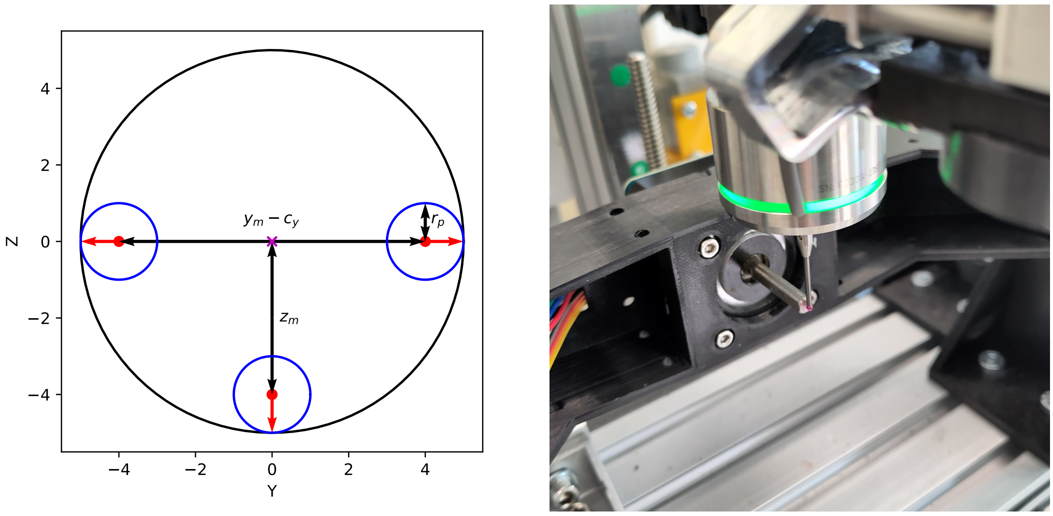

(a) (b)

Figure 5.9.: (a) shows the model concept for the measurement of the position of the A axis using a circle in the YZ plane. (b) is a capture from the active process of measuring one of the Y positions (y_{90}).

5.4.2. Machine Origin Calculation

We find the closest approach of both axes and define the point on the B axis as the (pseudo-)intersection (see figure 5.13). The calculation has been implemented in GCode directly on the printer, as such a simplistic formula was chosen to find the closest approach. Equation 5.7 shows the approach. For the calculation first an orientation vector n perpendicular to both A_{dir} and B_{dir} is found. The line describing the closest approach must be linearly dependent on n. The points on the lines are computed by first finding the scalars t_1 and t_2 which in turn can be used to shift the points on the lines according to the line formula. The approach is limited to non-parallel lines, which are unlikely given the real-world measurements and context of the A and B axes. The offset of the B axis position in the current frame is B''_{pos}, which has to be corrected to set it as the 0 point. A^B_{pos} describes the position of the A axis in the corrected frame. Further, calibrated systematic offsets $x_{bias}, y_{bias}, z_{bias}$ of the 3D touch probe are compensated in this step. As we defined all biases as additive, they can directly be added to the measured B axis position B_{pos} to shift it to the real position of the axis. For the A axis position the z_{bias} is applied to the Z component of A_{pos} to adjust the Z height to the experimentally verified value. For the A measurement, the X position is not adjusted as it a commanded value and not measured. In contrast to the B axis position, for the A axis the y_{bias} is subtracted from the Y position of the measured point. In the case of the B axis the outside of the metal axle of the B motor is measured. For the A axis an internal diameter of a circle is determined. Consequently, the bias in the Y values will have influenced the measurements in the opposite direction. Additionally, an offset in the Z rotation angle found using the A axis orientation test (see section 6.2.2) is compensated for. The A_{dir} vector is

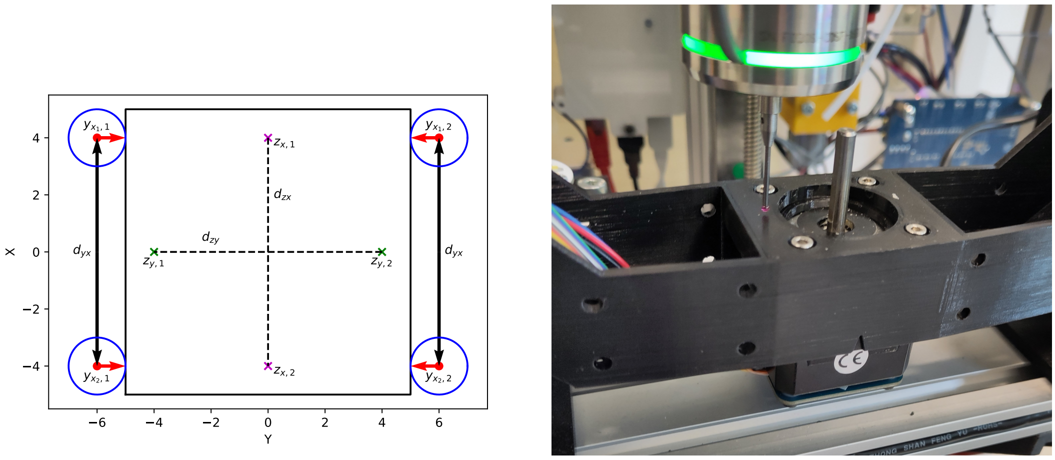

(a) (b)

Figure 5.10.: (a) shows the model concept for the measurement of the direction of the A axis viewed from the top. (b) is a capture from the active process of measuring one of the Z positions on the top surface ($z_{x,1}$).

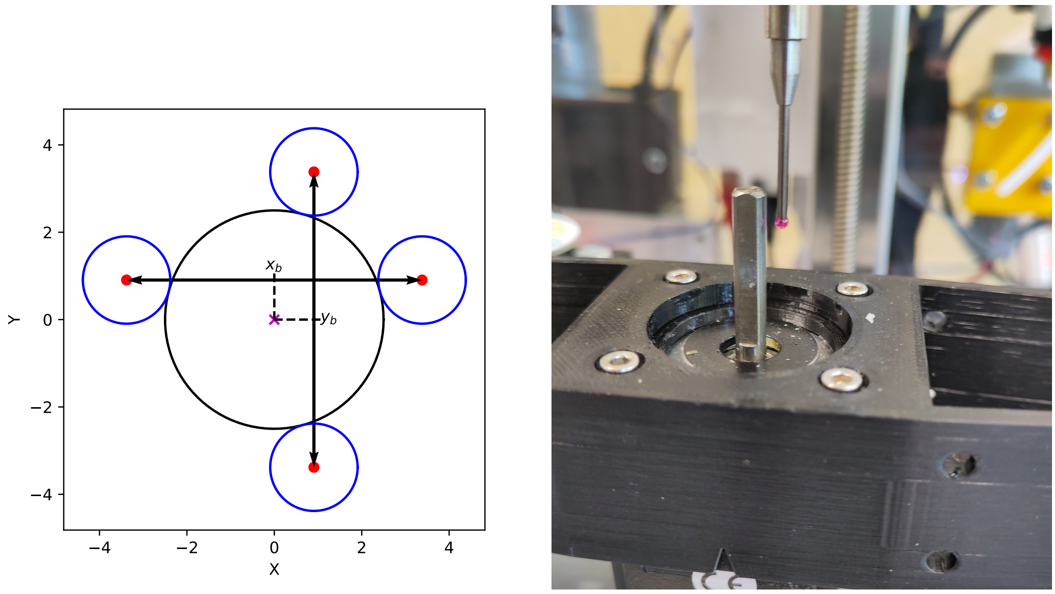

(a) (b)

Figure 5.11.: (a) shows the model concept for the measurement of the position of the B axis by constructing a cylinder shown from the top. (b) is a capture from the active process of measuring one of the Y positions of the B axle (y_{p_1}).

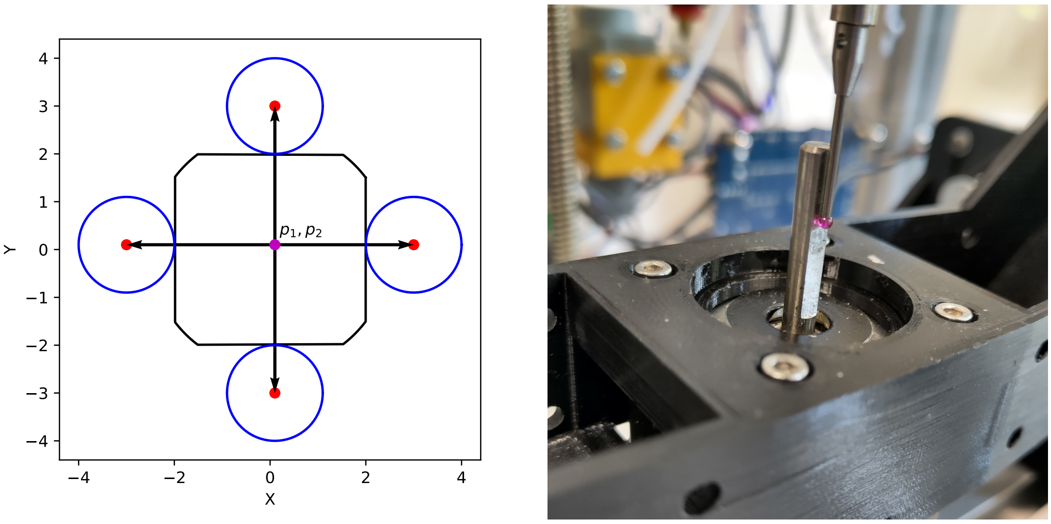

(a) (b)

Figure 5.12.: (a) shows the model concept for the measurement of the direction of the B axis viewed in the XY plane for one height. (b) is a capture from the active process of measuring one of the side points of the B motor axle ($p_{z2,1}$).

rotated in the Z plane by the correction angle $\alpha_{A,z}$ using a standard 3D rotation matrix.

$$\begin{aligned}
R_z(\theta) &= \begin{bmatrix} cos\ \theta & -sin\ \theta & 0 \\ sin\ \theta & cos\ \theta & 0 \\ 0 & 0 & 1 \end{bmatrix} \\
A'_{dir} &= A_{dir} \cdot R_z(\alpha_{A,z})^T \\
A'_{pos} &= A_{pos} + [0, -y_{bias}, z_{bias}] \\
B'_{pos} &= B_{pos} + [x_{bias}, y_{bias}, z_{bias}] \\
n &= A'_{dir} \times B_{dir} \\
t_1 &= \frac{(B_{dir} \times n) \cdot (B'_{pos} - A'_{pos})}{n \cdot n} \\
t_2 &= \frac{(A'_{dir} \times n) \cdot (B'_{pos} - A'_{pos})}{n \cdot n} \\
A''_{pos} &= A'_{pos} + t_1 A'_{dir} \\
B''_{pos} &= B'_{pos} + t_2 B_{dir} \\
A^B_{pos} &= A''_{pos} - B''_{pos}
\end{aligned} \tag{5.7}$$

For our printer the most significant rotation proved the A axis in the Z plane. The angle is approximated by $\theta = sin^{-1}((A'_{dir}).y)$.

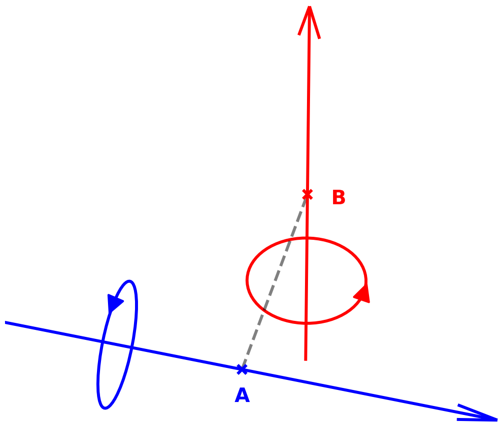

Figure 5.13.: Schematic of the axes oriented in 3D space with the closest approach shown by the gray line.

The step-by-step approach is directly based idea of the line axis model and is not able to directly determine parameters beyond it.

6. Evaluation

We consider the evaluation of the results in two groups. The internal validation is testing the precision of measurements directly from the printers sensors. The external validation is based on the examination of printed test objects. A short overview discussion is held after the individual measure series have been evaluated.

6.1. Internal Validation

For the internal validation of measurements, repeated measurements are analyzed using statistical means.

6.1.1. Hardware Validation

The hardware of the printer was also tested using mostly direct comparisons of repeated measurements.

Probe Analysis

The 3D touch probe (See section 4.2.3) has been analyzed with regard to trigger consistency and hysteresis. Additionally, using known objects the dimensional accuracy of measured vs known size has been calculated to allow for compensation of systematic errors. All of these measurements were collected using the *probe_measure* script with 10 samples and a step size of $0.01mm$. The figure 6.2 shows the consistency and hysteresis results. Using the trigger positional value as the basis the consistency was further analyzed statistically (see table 6.1).

The 3D touch probe shows standard deviations in the single digit μm and maximal differences in the low tens of μm (see table 6.1). $Y-$ as the probing direction shows the most movement

Axis	STD	Max Difference
$X+$	0.003	0.010
$X-$	0.005	0.010
$Y+$	0.000	0.000
$Y-$	0.006	0.020
$Z-$	0.005	0.010

Table 6.1.: Table showing the consistency results for each axis direction defined by standard deviation (STD) and the maximum value difference in mm.

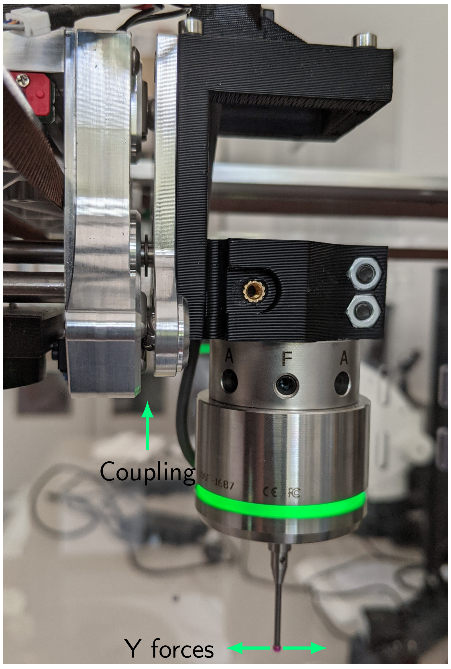

Figure 6.1.: Side view of the touch probe showing the suspected error-inducing Y forces visualized. The coupling to the tool is particularly weak to Y direction forces.

in the values, which is explainable by the toolchanger[38] holding the tool into this direction with the least support, introducing errors into the system (see figure 6.1).

The dimensional bias was calculated by probing the flat side of the B axle from all X and Y directions with approximating the side to point exactly into the dimensional axes. The resulting object has a size of $4mm$, resulting in the additive compensation values of $c_x = 0.326,\ c_y = 0.453$ indicating that the measurements result in smaller objects.

Further the hysteresis of the probe was characterized in figure 6.2. The probe was moved in the direction in $10\mu m$ steps (see section 5.1.5). All directions showed a hysteresis of $< 100\mu m$. It should be noted, that the CoreXY kinematics potential backlash could be a contributing factor to the hysteresis results. The hysteresis results themselves have not been used in the calibration of the printer, but the measurements enabled most tests relating to the probe's reliability.

Pick Up Repeatability

The repeatability of the tool changers pickup was tested by using the 3D probe tool (See section 4.2.3) and measuring the X, Y and Z value of surfaces on the B axis spindle. Over 10 tool pick up and return operations resulted in a $\sigma \approx (0.007, 0.005, 0.0007)$ and a maximal difference of $(0.02, 0.01, 0.002)$. The resulting 3D coordinates were plotted in figure 6.3. Generally the result of the statistical analysis show combined effects of the 3D probe reliability combined with differences caused through multiple pick-ups.

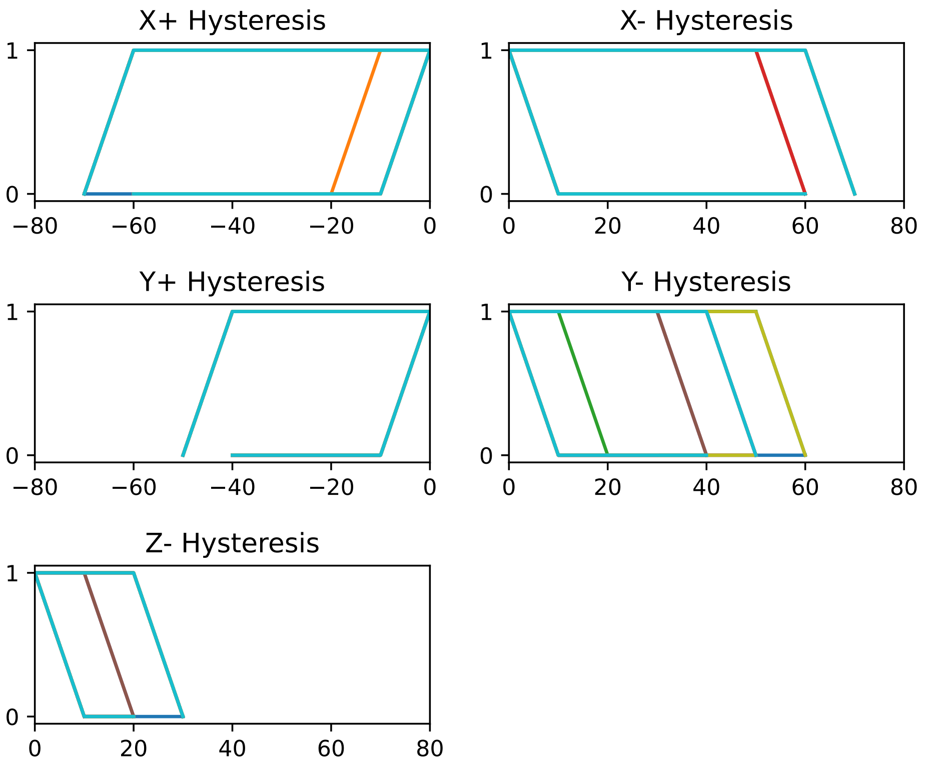

Figure 6.2.: The measured hysteresis and trigger consistency of the 3D touch probe

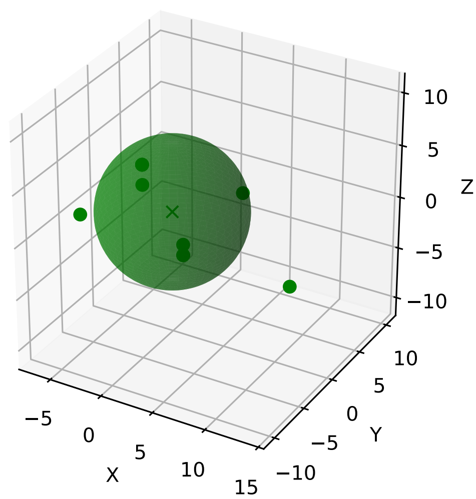

Figure 6.3.: 3D Plot of the Pick-up test results. All units in μm and the mean set as $[0, 0, 0]$. The green sphere specifies the maximum σ of all axes.

The combined test of the toolchanger pick up system and the touch probe showed no significant difference from tests where the probe was tested repeatably without new pick-up sequences (see section 6.1.1). This indicates the reliability of the toolchanger system is as advertised by E3D[30], especially when considering the high length of our tools.

Print Bed Measurements

The figure 6.4 shows a visualization of the measured bed heights according to the approach described in section 5.1.4. The resulting direction of the B axis based on the two measurements is $\approx [2.19 \cdot 10^{-3}, -1.64 \cdot 10^{-3}, 0.99999626]$. The normal of the print bed with B considered pointing exactly upwards results in $\approx [7.819 \cdot 10^{-4}, 3.227 \cdot 10^{-4}, 0.999999642]$ In general two effects can be observed in the data. A general pitch to the B axis itself and also an incline to the bed itself as the rotation reduced the slope of the bed. As the orientations are measured in the 3D printer's kinematic frame. Consequently, other effects of the XYZ-gantry not being aligned perfectly could be at play. The irregular low spots are screw holes in the surface of the bed for attaching other assemblies (see figure 4.2).

A Axis Homing

The homing of the A axis is described in the section 5.1.2. During the measurement of the A axis direction, the rotation of the A axis is also checked. To ensure it is at the correct 0 position the change in Z over the Y direction is measured. The values were measured in two independent runs of 20 measurements with a full printer restart in between. For the first run $m_{zy} \approx 9.172 \cdot 10^{-4} \pm 6.066 \cdot 10^{-4} (2.687 \cdot 10^{-3})$ is the result given in the $mean \pm std(diff)$ format. The second run gave $m_{zy} \approx 3.733 \cdot 10^{-3} \pm 2.995 \cdot 10^{-4} (9.064 \cdot 10^{-4})$.

Using the result for the B axis orientation (see table 6.2) the slope of Z in the Y direction has been calculated. The formula used was $m_{zy} = tan(cos^{-1}(B_{dir} \cdot [0, 0, 1]))$ with B_{dir} signifying the B axis orientation vector. The results have been $4.1 \cdot 10^{-3}$ and $5.3 \cdot 10^{-3}$ for the first and second run respectively.

The homing of the A axis showed passable levelness of $0.213°$ which is a change of $37 \mu m$ in height per $1cm$ of movement in the Y direction (see section 6.1.1). The value is higher than desired but still in a usable range for smaller objects with the layer height of $0.2mm$. Calculating the slope based on the B axis orientation yielded results for both runs similar to the average of the second run. This indicates the actual slope might be closer to the worse result in both cases. It must be noted, that the B axis direction can include additional factors based on the mount of the stepper motor.

The A axis was first calibrated using results similar to the first measurements, where the axis seemed to be correctly oriented. The second series shows a significant slope, which could be changed by directly adjusting the zero point setting.

A Axis Scaling

The A axis scaling has been measured according to the procedure described in section 5.1.7. It was found that the $-90°$ position showed good results with an offset of $\approx -0.126°$. The

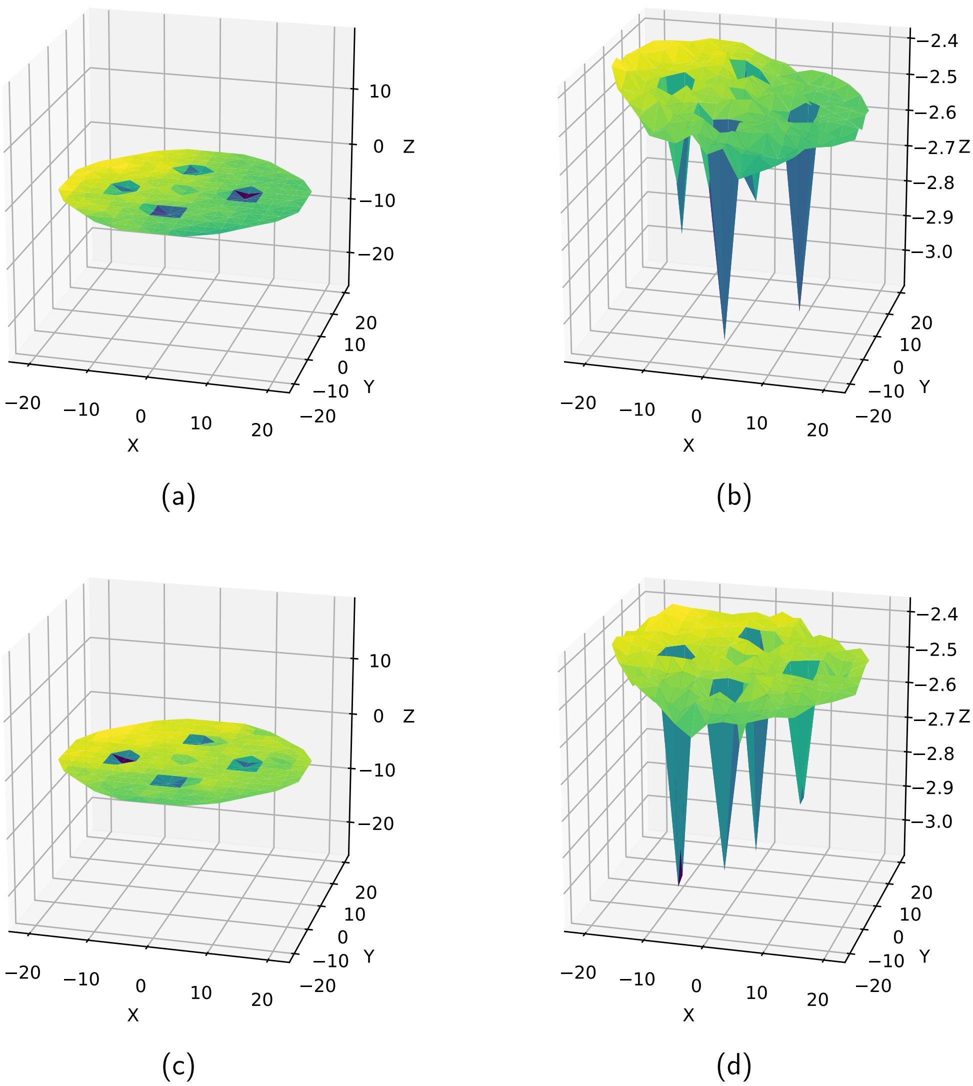

Figure 6.4.: Height visualization of the metal print bed as probed. (a) and (b) show the bed in the 0° position. (c) and (d) show the bed in the 180° position of the B axis. (a) and (c) are visualizations with all 3D axes having the same scale, while (b) and (d) show the same data with the Z axis scaled to the data.

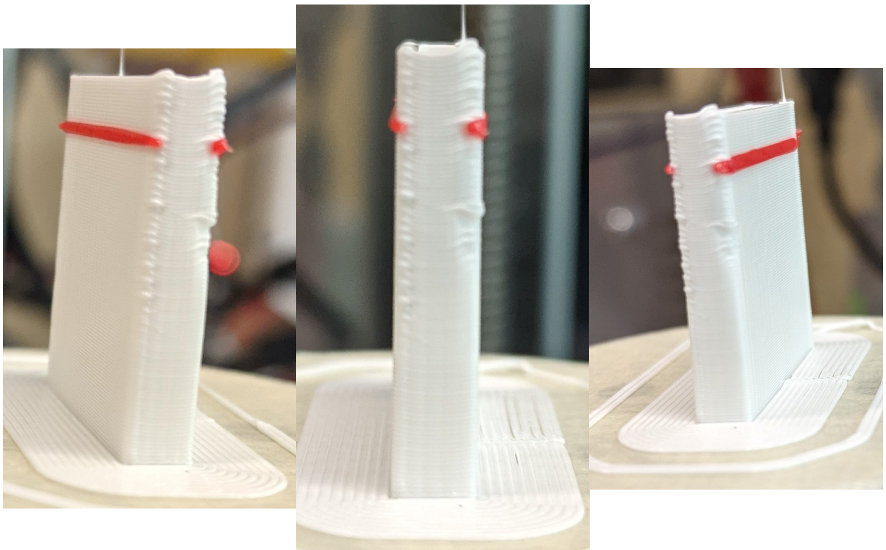

Figure 6.5.: The difference in the extrusion width the A position test without Z shift compensation is shown. The left side is too far from the object, showing a line deposited using gravity. The right side expresses a thick line with the nozzle being to close to the object. The front view of the test indicates a correctly calibrated distance of the A and B axes.

positive direction resulted in an angular error of ≈ -0.63°, significantly impacting the position of rotated objects. After adjusting the scaling of the A axis the errors changed to ≈ -0.138° and ≈ -0.143°. The result improved the behavior to an acceptable level. Having the same error on both sides shows potential in changing 0 point position. Further, tuning of these values could help to further improve the capabilities of the printer. Though the precision of the system could prove to be the limiting factor, especially between restarts.

A Axis Z Shift

The A axis shift between the step-by-step result in values of $z_d \approx 0.13mm$. Using this values as the post-processing step enabled the printing of the final integrated result (see figure 6.20).

Without the shift the extrusion width showed significant variations between the ± 90° positions of the A axis (see figure 6.5). A result with compensation is shown in figure 6.14

6.1.2. Sphere Measurement Validation

The center of the sphere object has been measured 11 times in the same position. The values are plotted in figure 6.6. A variation of up to 1 mm can be observed in the Z position of the center point. The fitted radius of the sphere fluctuated for $\approx 0.985mm$ with a standard deviation of $\approx 0.334mm$, explaining the movement in the Z coordinate. Given the top of the sphere is measured with low Z height variation, noise has strong effects of the fitted curve of the sphere.

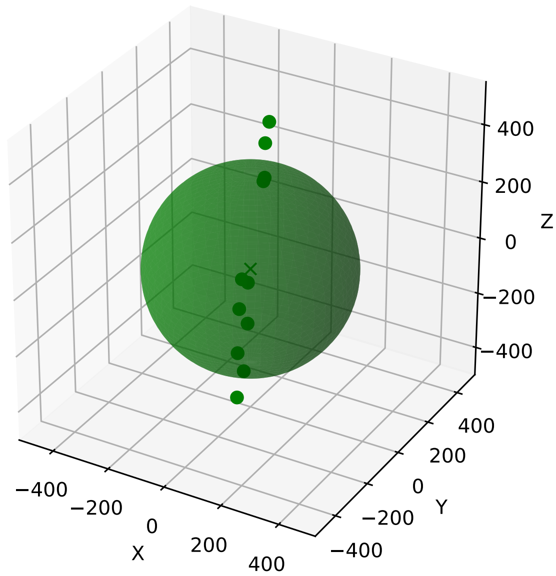

Figure 6.6.: Sphere center measurement results plotted in 3D space. The x marks the mean and is defined as 0,0,0. The green sphere visualizes the standard deviation of the Z coordinate. All units in μm.

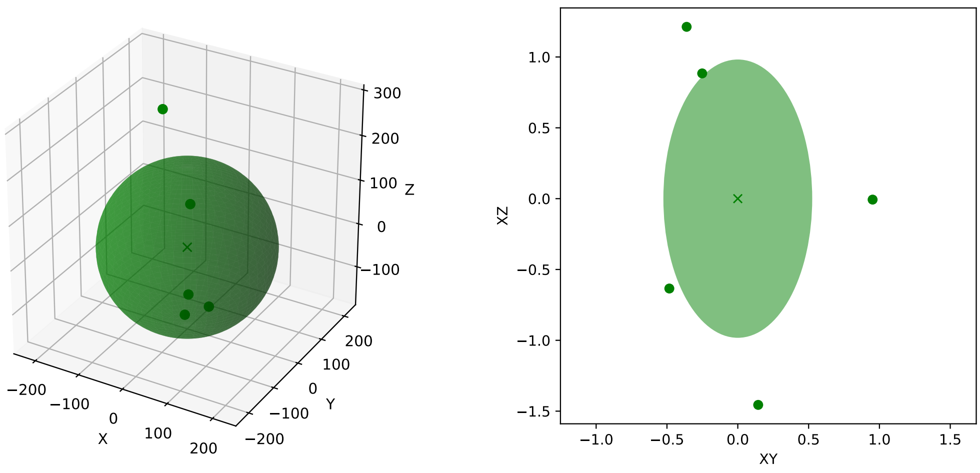

(a) (b)

Figure 6.7.: A axis results using the sphere approach. (a) shows the position of the A axis in μm. The mean of the values is set as 0,0,0. The sphere specifies the highest standard deviations of the X, Y or Z component. (b) plots the angular difference to the mean orientation vector in degree in the XY and XZ planes. The ellipse represents the component standard deviations.

Five measurements of the A axis position and direction were performed using the sphere approach. The resulting axis components are visualized in the figure 6.7. Both the positional and directional values show significant movement between measurements. The position's Z component expresses a standard deviation of $\sigma \approx 0.18mm$.

The sphere approach showed signs of working quite well with the small integrated Z probe of the E3D toolchanger [38]. Though due to the limited clearance of the switch only a small area is being accessible to be probed. Using no additional hardware presents advantageous as the implementation of the approach would create few hurdles. Further the standard Z switch is very precise ($\lessapprox 10\mu m$) and cheap. Usage of the more versatile 3D touch probe (see section 4.2.3) proved problematic, as the touch force for the 3 spatial directions (esp. the Z axis) is designed to be asymmetric. The forces potentially would have to be characterized to use the measured values from the probe as the sphere surface applies a 3D force when probed in the Z direction. Further the noise of the measurements proved to be high, as small changes in coordinates could change the surface direction of the sphere greatly. A problem proved the manufacturing of a good sphere object in our lab which is spherical and of high surface quality. This could be addressed by creating a design using standard metal bearing balls. Lastly using a sphere directly on the axes only works reliably for inaccurate or skewed axes. The rotational symmetry of the sphere gives very similar results for axes going through the center with random noise drowning out the actual measured structures. This was the case for the B axis. Further extension of the approach could prove valuable given changes to the

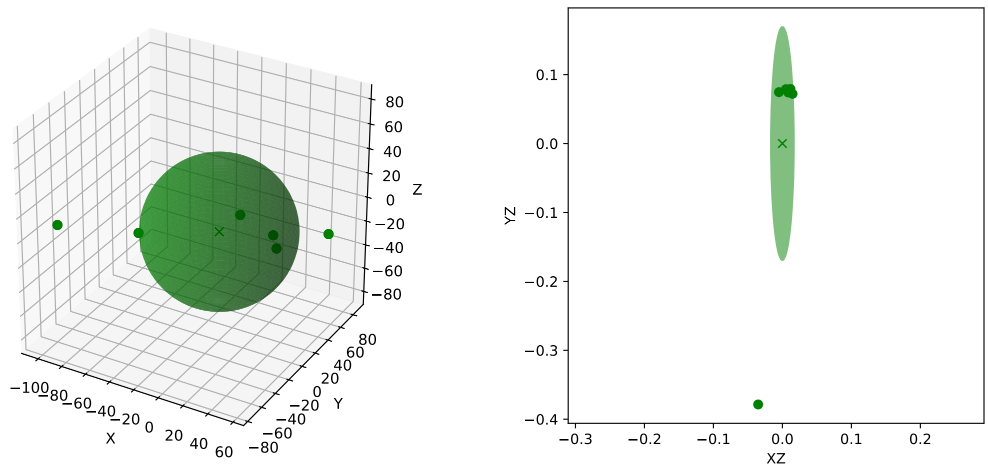

(a) (b)

Figure 6.8.: Cross center and normal measurement results plotted in 3D space. (a) shows the position of the center in μm. The x marks the mean and is defined as 0,0,0. The sphere specifies the highest standard deviations of the X, Y or Z component. (b) plots the angular difference to the mean orientation vector in degree in the XZ and YZ planes. The ellipse represents the component standard deviations.

object geometry are made which would remove the rotational symmetry.

6.1.3. Cross Measurement Validation

The cross object has been measured for 6 times in the same position. The result is shown in the figure 6.8. Both the orientation and center position are show quite stable results, especially when compared to the sphere center measurements (see figure 6.6). Through center's x component shows a standard deviation of $\sigma \approx 56.7\mu m$ with differences up to $\approx 155\mu m$.

Two measurements for the B axis were performed and compared (see figure 6.9). Although too few results to reach confident conclusions, an idea of the expected behavior can be conveyed. The B positions show a difference of $\approx 115\mu m$ in the Y coordinate, indicating better repeatability than the sphere approach. Though the step-by-step approach reduces this error by a factor of 3 (see table 6.2). The B orientation result is comparable to the step-by-step approach, showing stability up to the 4th digit of the decimal.

The calibration cross approach has been developed quite far before being abandoned. The main problem was the process not working well for the measurement of the A axis. Test probes from the Z direction, which stressed the B axis, were able to move the B axis motor, forcing it to lose steps. Further the measurement procedure was quite slow, as many points were collected. The further development of the approach could address these two concerns.

A further problem is the manufacturing of a durable and accurate cross shape in our lab, as mostly only 3D printing technology is available. This combines with the problem of securely

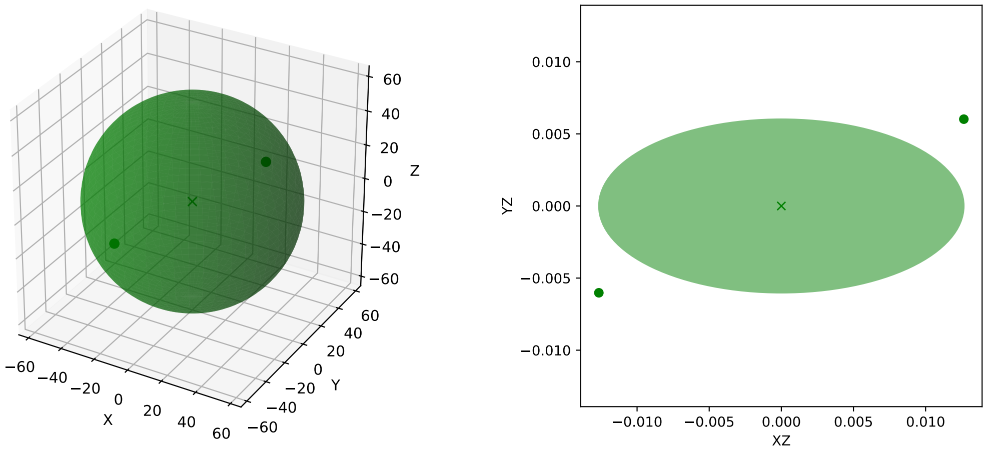

(a) (b)

Figure 6.9.: B axis results using the cross approach. (a) shows the position of the B axis in μm. The mean of the values is set as 0,0,0. The sphere specifies the highest standard deviations of the X, Y or Z component. (b) plots the angular difference to the mean orientation vector in degree in the XZ and YZ planes. The ellipse represents the component standard deviations.

and repeatably mounting the cross on the B axis spindle. We had problems with movement in the mount under probing loads.

As the processing of the cross measurements relies on fitting algorithms, spatial projections and transformations, a more powerful calculation backend like OctoPrint [33] with Python is needed rather than extended GCode.

6.1.4. Step-by-step Measurement Validation

In this section the results of the step-by-step approach's axes measurements are compared to themselves and between two different runs. The axes were measured according to the approach described in section 5.4.1 without finding the closest approach of the axes.

Within Runs

For the internal validation of the measurements, repeated data-points were collected within one start up and homing sequence of the printer. The measurements were repeated twenty times and their results analyzed using Python. The results are show in the table 6.2 and visualized in figure 6.10

Measurements of the axis positions show deviations between $\pm 8\mu m$ to $\pm 20\mu m$ with maximum differences of $30\mu m$ to $56\mu m$ (see table 6.2). Given to accuracy of the printer axes of around $10\mu m$ the results are significant enough to change the final position of the print

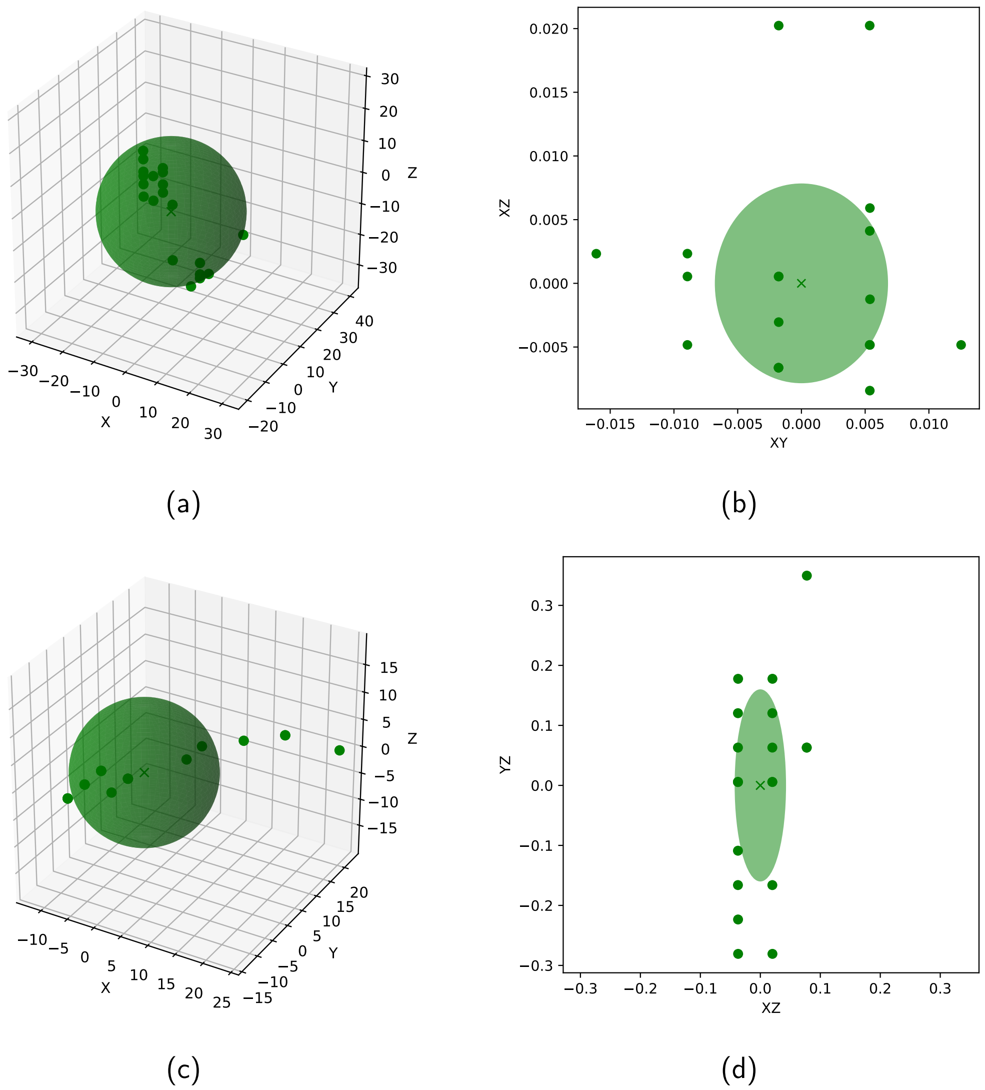

Figure 6.10.: Visualized results of the measurements for each axis and component. (a) shows the A axis position in μm. The mean is defined as $[0, 0, 0]$. The sphere shows the radius of the standard deviation based on the maximum σ of X, Y or Z. (b) plots the angular difference to the mean orientation vector in degree in the XY and XZ planes. The ellipse represents the component standard deviations. (c) and (d) show the same for the B axis respectively for the XZ and YZ planes.

Component	X	Y	Z
A Axis Position	$0 \pm 0(0)$	$-0.241 \pm 0.015(0.055)$	$-0.214 \pm 0.02(0.056)$
B Axis Position	$-0.114 \pm 0.008(0.03)$	$0.068 \pm 0.012(0.035)$	$-10 \pm 0(0)$
A Axis Direction	$0.999 \pm 3.92 \cdot 10^{-6}(1.67 \cdot 10^{-5})$	$0.033 \pm 1.176 \cdot 10^{-4}(4.992 \cdot 10^{-4})$	$-4.591 \cdot 10^{-4} \pm 1.359 \cdot 10^{-4}(5 \cdot 10^{-4})$
B Axis Direction	$6.486 \cdot 10^{-4} \pm 7.268 \cdot 10^{-4}(2.005 \cdot 10^{-3})$	$4.1 \cdot 10^{-3} \pm 2.773 \cdot 10^{-3}(0.011)$	$1 \pm 1.256 \cdot 10^{-5}(4.05 \cdot 10^{-5})$

Table 6.2.: Results of the repeated axes measurements separated by axis and component. The absolute positions of the axes are expressed in the current, uncalibrated printer frame. Showing mean $\pm$ standard deviation (max difference between values). All positional values in millimeter and rounded to three digits after the period. The orientations are given as unit vectors. The X value of the A axis is an input and as such always 0. The same applies for the Z value of the B axis with it being set to -10 mm.

Component	XY	XZ	YZ
A Axis Direction	$\pm 0.007(0.029)$	$\pm 0.008(0.029)$	$\sim$
B Axis Direction	$\sim$	$\pm 0.042(0.115)$	$\pm 0.159(0.63)$

Table 6.3.: Results of the repeated axes direction measurements separated by axis. The values are expressed as $\pm$ standard deviation (max difference between values). All values given in degree and rounded to 3 digits after the period. XY, XY and YZ specify the rotation of the vector in the plane given from the mean orientation. ' ' marks planes, in which the vector elements are composed of small values and affected by noise such that the angular error poses no practical value.

head. Considering the central 1σ it only shows results at the limit of the kinematics. The nozzle used in the printer is a standard $0.4mm$ and a layer height of $0.2mm$ is used. A such the printer is expected to be usable with the accuracies achieved.

The orientations of the axes are generally quite stable as they incorporate many data points into one result. The variation in the orientation vector values range from the 10^{-6}th to the 10^{-3}th digit with most falling into the 10^{-4} category when considering 1σ (standard deviation). The total maximal difference lies between 10^{-5} to low 10^{-2} in the case of the B axis' Y component. Examining the variation in the B axis further, we approximate the angle change in relation to a vector pointing straight up. The change in Y equals to $\approx 0.63°$ of total variation in the Y orientation. A difference of up to $\pm 1mm$ per $10cm$ along the vector in the resulting Cartesian position. Further the result of the B axis orientation only based on Z probes of the print bed fall into 1σ of the step-by-step process. The notable exception is the Y components result which only matches the full spread of the values (see section 6.1.1).

Further, the directional values were analyzed for the angular deviation within the measurements (see table 6.3). The previously described effects are observed here with the B axis orientation showing significant variations. In contrast, the A axis results show a rather stable behavior.

This indicates problems with the measurements in the Y direction showing inconsistency a bit above the upper bound of what is acceptable as good.

Between Runs

In a second measurement series the printer has been restarted to collect data-points between two initialization states without adjusting the frame configuration. These were compared to the ones collected in section 6.1.4. The comparison plot is show in figure 6.11.

We detected significant differences between the measurements between the positional results of the axes between runs of the printer, showing unrepeatable homing behavior (See figure 6.10). Resulting from this the measurement procedure of the axes must be executed after every homing of the X, Y or Z axis. In a future iteration the measurement could be reduced to remeasuring the B axis positions and then recalculating the values.

6.2. External Validation

To verify the results of the measurements real world tests were run. All of these tests use the extruders as the main tools. The shape of the extruded material indicates the quality of the calibration. Using the external validation procedures the measured results of the axes components were (mostly) tested independently.

The real world results of the tests are shown in the figures 6.14, 6.15, 6.16 and 6.18.

Three of the four tests use a base object, which is printed using standard 3D printing techniques (see figure 6.13). A line is then printed onto the base object using 5 axis movements. The base object is printed using one extruder with white PLA material, while the lines are printing using the second tool with red PLA filament.

To verify the results a visual inspection of the objects was performed. For a more accurate determination calipers were used. Though often the position of the line and the width of the extrusion were not easily separable.

6.2.1. A Axis Position Test

The position of the A axis is tested by printing a straight line onto a flat object in the $A \in \{90°, -90°\}$ positions (see figure 6.14). The lines are expected to be at the same height on the object. After the two lines have been printed, the height on the actual object could differ (see figure 6.12), indicating a Y offset of the position of the actual A axis. The process doubles the calibration error, as the error gets applied two times, once per rotation. Further the extrusion width of the lines can be checked to test for possible Z offset errors. Errors in the shift of the B axis also result into different widths on the sides.

The tests of the A position show a good calibration of the Y coordinate of the axis, as the lines are at the same height. This can be visually identified by examining the layer lines on the print, which have a height of $0.2mm$. The height of both lines has also been measured using as caliper resulting in $\approx 2.6mm$ distance from the top on both sides. The measurement is performed using the bottom depth probe by hooking it to the extrusion. The caliper tests are not very precise in this use case.

Further the equal extrusion shows good Z direction results given the Z wobble adjustment has been applied (see section 5.1.8).

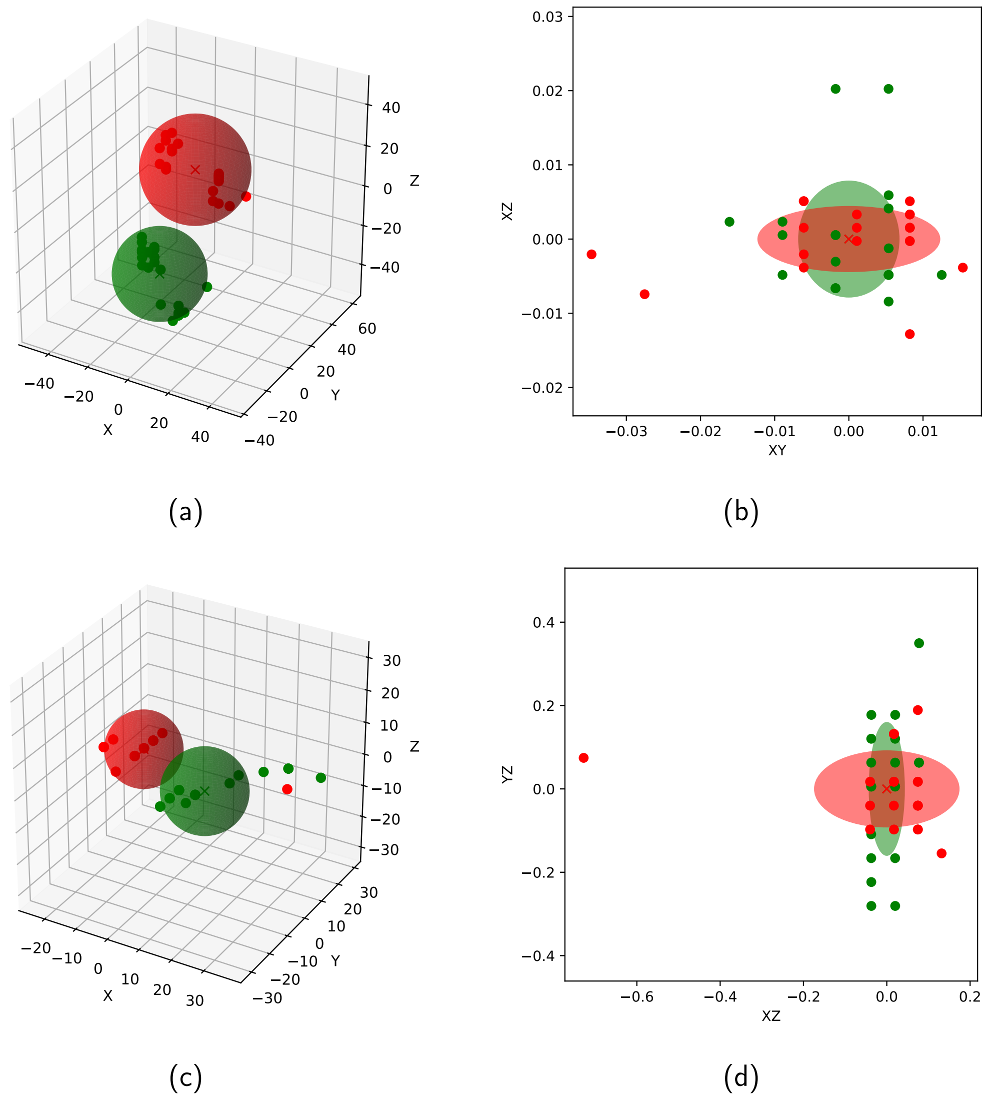

(a) (b) (c) (d)

Figure 6.11.: Visualized results of the measurements for each axis and component between two printer restarts. The datasets are separated by color. (a) shows the A axis positions. All units in μm. The mean of both measurement series together is defined as $[0, 0, 0]$. The spheres show the radius of the standard deviation based on the maximum σ of X, Y or Z. (b) plots the angular difference to the mean orientation vector in degree in the XY and XZ planes. The ellipse represents the component standard deviations. (c) and (d) show the same for the B axis respectively.

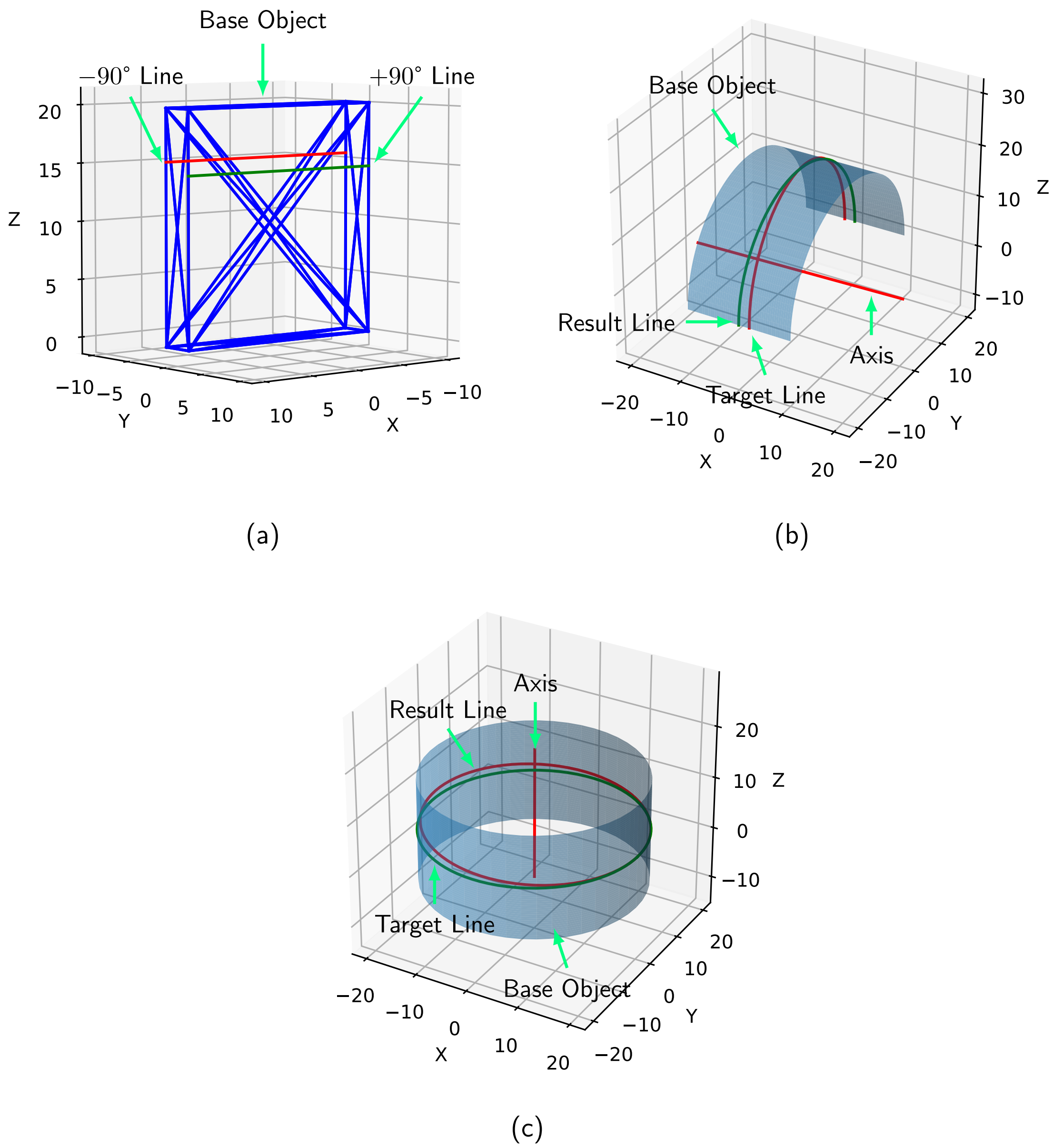

Figure 6.12.: Simulated error cases with exaggerated possible deviations. All units in mm. (a) shows the A axis position test with a shifted position indicated on the object surface by the differential height of the lines. (b) displays the A axis orientation test. The green line shows the target line and the red surface line a possible error case where the ends are shifted. (c) a test for the B axis orientation. In green is the target line and red a simulated actual result in the case of deviations.

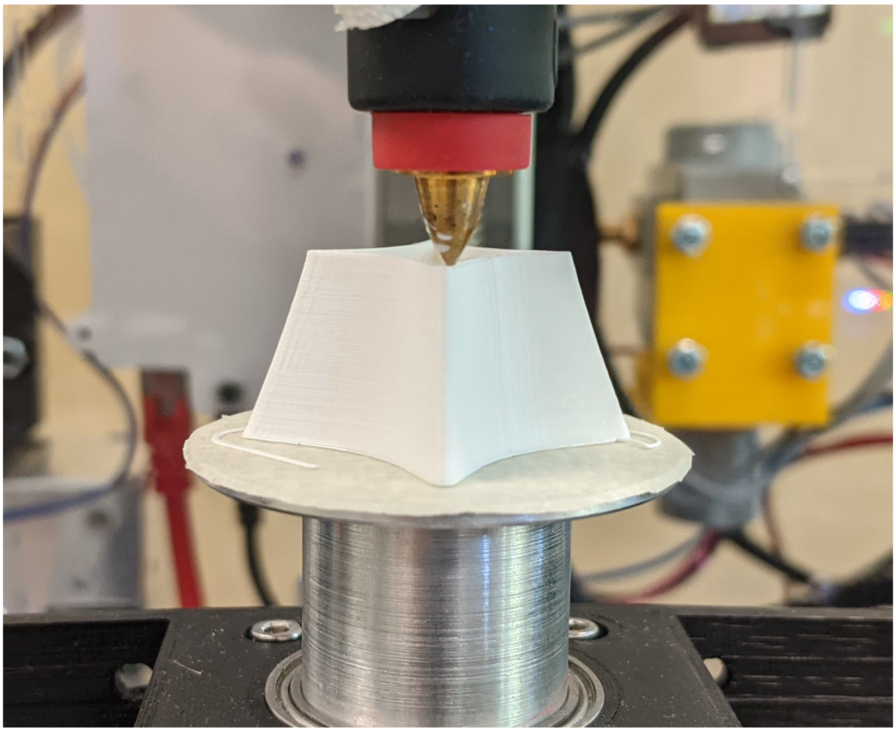

Figure 6.13.: Example printing process of a base object.

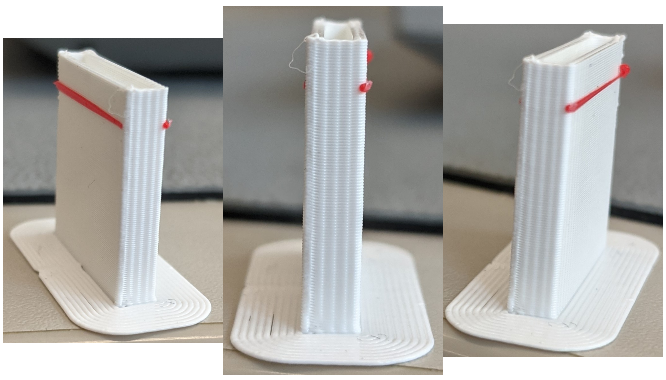

(a)

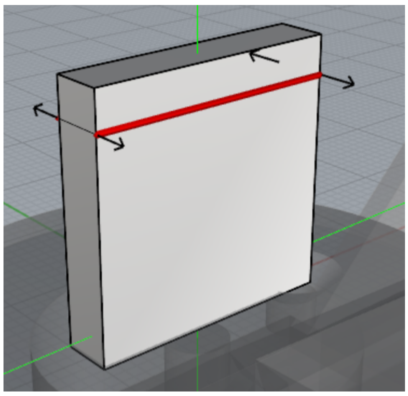

(b)

Figure 6.14.: Test for the position of the A axis. (a) shows a calibrated result of the test. (b) shows the Rhino 8 view

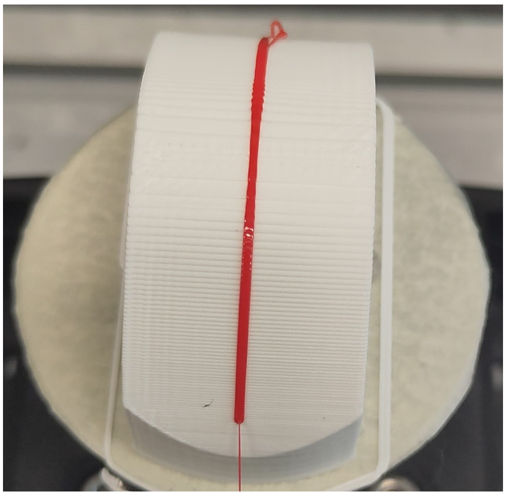

(a)

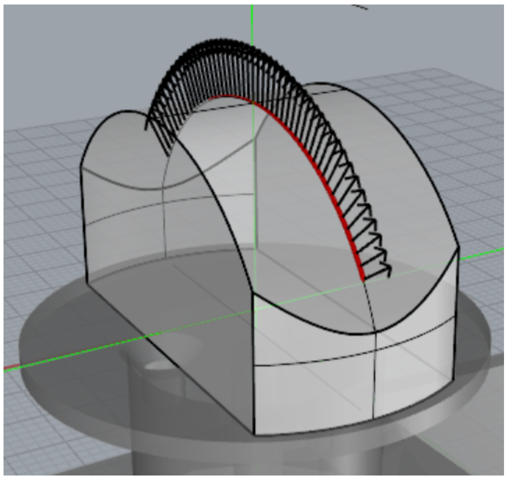

(b)

Figure 6.15.: Test for the direction of the A axis. (a) shows a calibrated result of the test. (b) shows the Rhino 8 view

6.2.2. A Axis Orientation Test

To test the orientation of the A axis a surface slice of a cylinder is first printed using the usual 2.5D process. A centered, straight line is drawn onto the surface, using the A axis in the main movement (see figure 6.15). The centering and straightness of the line indicates the quality of the calibration, as wrong angles will produce crooked lines (see figure 6.12). The test responds best to rotations in the Z plane, as rotations in the Y plane would change the position of the extruder on the surface symmetrically. Using this an error in the Z angle of the A axis measurements has been found. The line on the surface was approximated to have a length of 40 mm. Using calipers the distance of the line ends to the side of the objects has been measured. This resulted in an error slope, which indicated an orientation error of $-0.258°$ in the Z plane. The value is compensated for by the $\alpha_{A,z}$ correction factor in the origin calculation (see section 5.4.2). Other rotational errors have not been separated in this measurement, though in practice to assumption of only having Z rotations has been sufficient.

The orientation test of the A axis resulted in a visually perfect line. Using calipers a measurement from the side to center extrusion line resulted in equal distances at both ends with a precision of $< 0.1mm$ between data points.

6.2.3. B Axis Position Test

For the B Axis Position Test the compensation of B axis rotations was tested. A rotation of the B axis consists of a rotation of the print bed. The print head was moved to compensate for this such that a straight line would be drawn on the surface. Small deviations of the calibrated position would show up as bent lines. Using a simulated execution for comparison allows for direction identification of the positional errors.

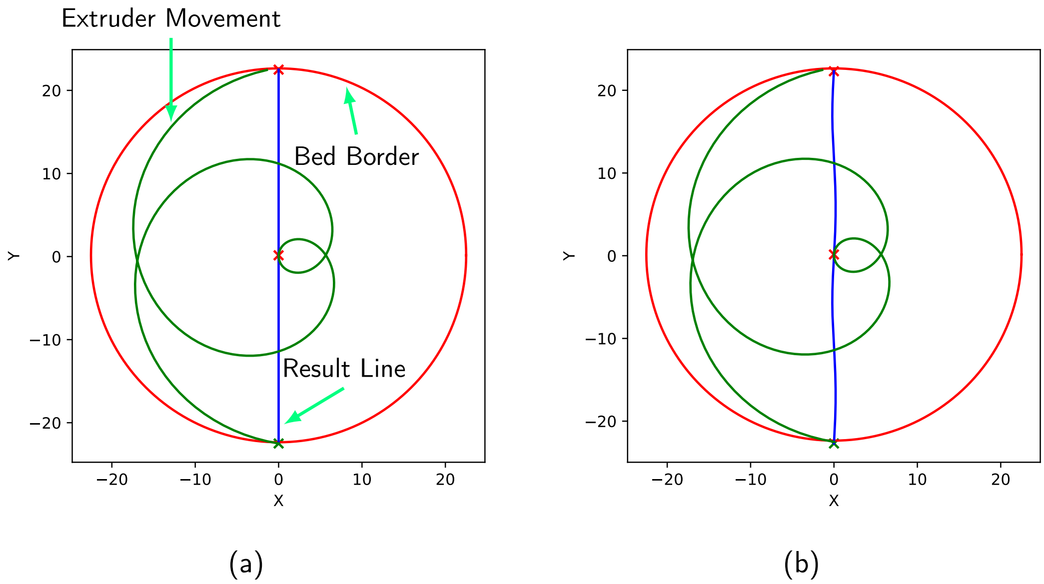

Figure 6.16.: Simulated test for the position of the B axis. The blue line is the resulting line by performing the movements of the green line and simultaneously rotating the B axis two revolutions. (a) shows the optimal result of a straight line (b) shows the expected result with a Y offset of $-0.2mm$, changing the straight line to a waving line

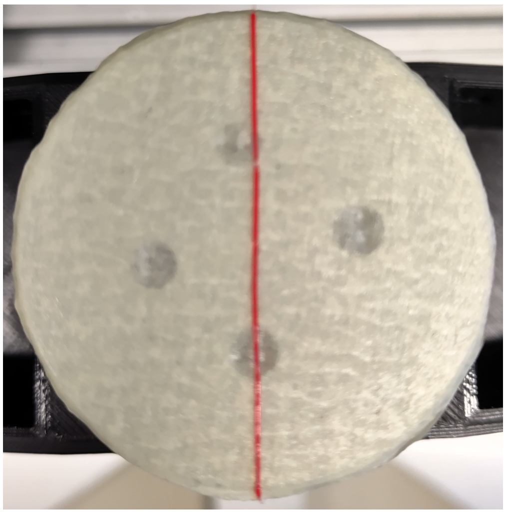

(a)

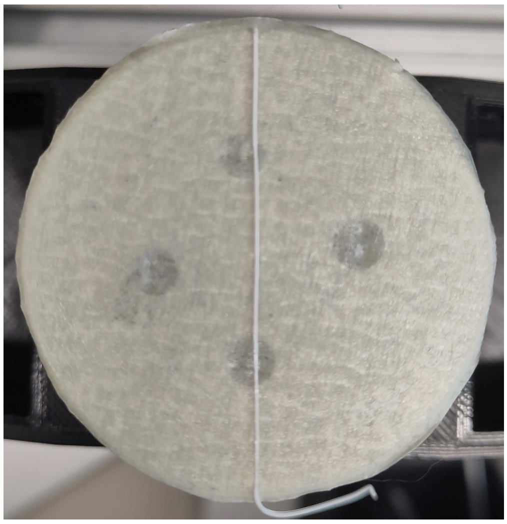

(b)

Figure 6.17.: Comparison of the extruder calibration using the B position test. (a) shows the extruder used for most tests with red filament. This further represents the B axis position test result. (b) shows a result of the extruder printing the white base objects.

The B axis position test was also performed using the second extruder to compare the alignment of the extruders. The test results are shown in figure 6.17.

The position of the B axis is almost perfectly captured as the line is close to completely straight on the print bed. Using an interactive overlay of the simulated result line, an approximate B offset of $x_{off} \approx -0.045, y_{off} \approx -0.025$ has been found to match. Further the comparison of both extruders shows two identical results, confirming the alignment of the hot-ends. The result is within the expected run to run position precision of the B axis position measurement (see table 6.2).

6.2.4. B Axis Orientation Test

The orientation of the B axis is tested by drawing a line on a cylinder surface by only rotating the B axis (see figure 6.18). For good calibration values a constant distance of the line from the edge of the cylinder is expected, while an offset would introduce a shifted line (see figure 6.12).

The test of the orientation of the B axis did not result in visible or measurable inaccuracies. Though this test is not as sensitive to errors as the others.

6.2.5. Integrated Test

In an integrated test the calibration quality is tested by using an example object with complex geometry requiring simultaneous A and B axes movement. A circle is projected from the top

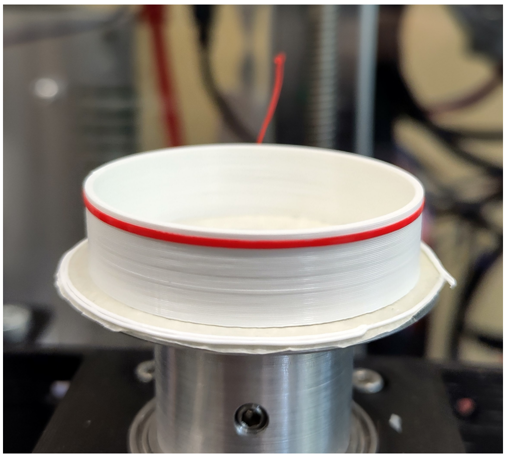

(a)

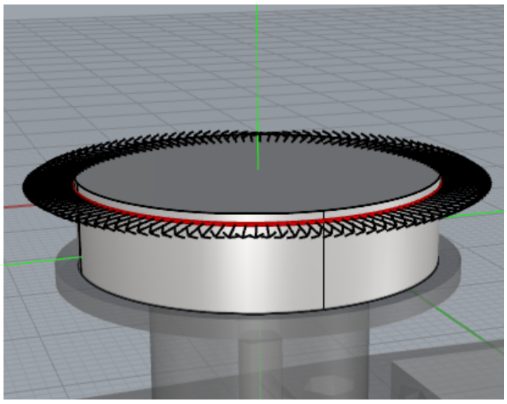

(b)

Figure 6.18.: Test for the direction of the B axis. (a) shows a calibrated result of the test. (b) shows the Rhino 8 view

such that movements of the A axis between $90°$ and $0°$ are required to draw on the sides and the top (see figure 6.19). The quality of the calibration can be judged by the extrusion quality of the circle line. Especially factors like how continuous the extrusion is, how consistent the width is and if the base object surface has been melted by the hotend. A printing process of such an integrated test can be viewed under `https://youtu.be/QCpKqnp3P4I`.

The real world quality of the results was also tested in a combined test object requiring multiple 5 axis movements (See figure 6.20).

The projection of a line onto a more complex object tests all the calibration settings together. The starting point of the print to the right of the image has imperfections. The line printed on the objects surface is securely attached to the object. Although some variation of the printer nozzle to the surface can be seen in the extrusion width, the nozzle has not scarred the surface. Additionally, the extrusion line of the plastic is mostly continuous. These properties were also confirmed in repeated tests, with slight variations of the quality. The presented result should represent the average case. Using the positional calibration of the B axis 0 point, but disregarding the A axis offset and rotation, results in a print with rotated lines and damage to the surface of the object.

6.3. Result Discussion

6.3.1. Requirement Fulfillment

The requirements were:

- **Reduce human involvement:** little human action required
- **Time Constraint:** less than 15-30 minutes

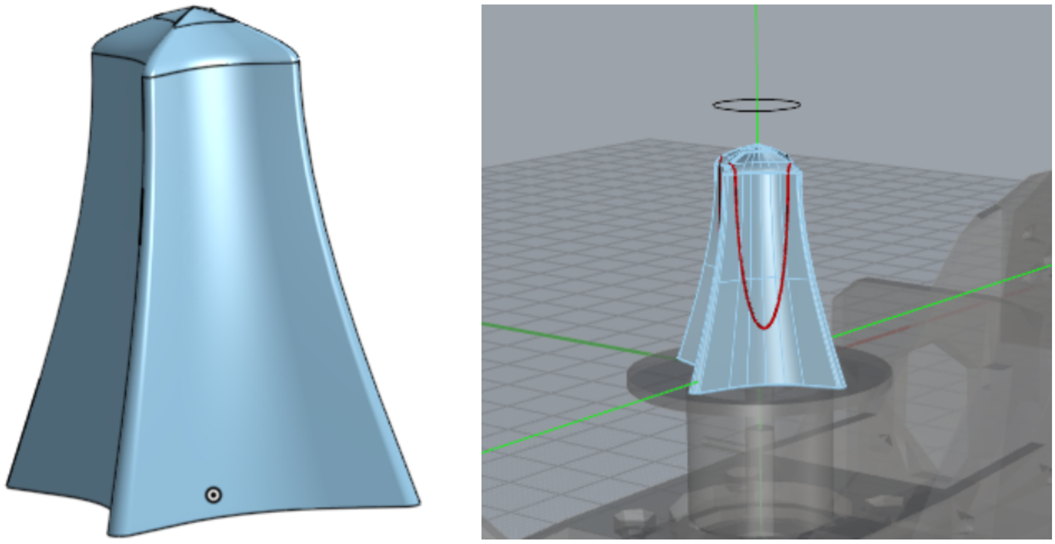

(a) (b)

Figure 6.19.: Integrated test of A and B axis movements (a) shows the basic test model (b) shows the Rhino 8 view with the target path in red on the object's surface

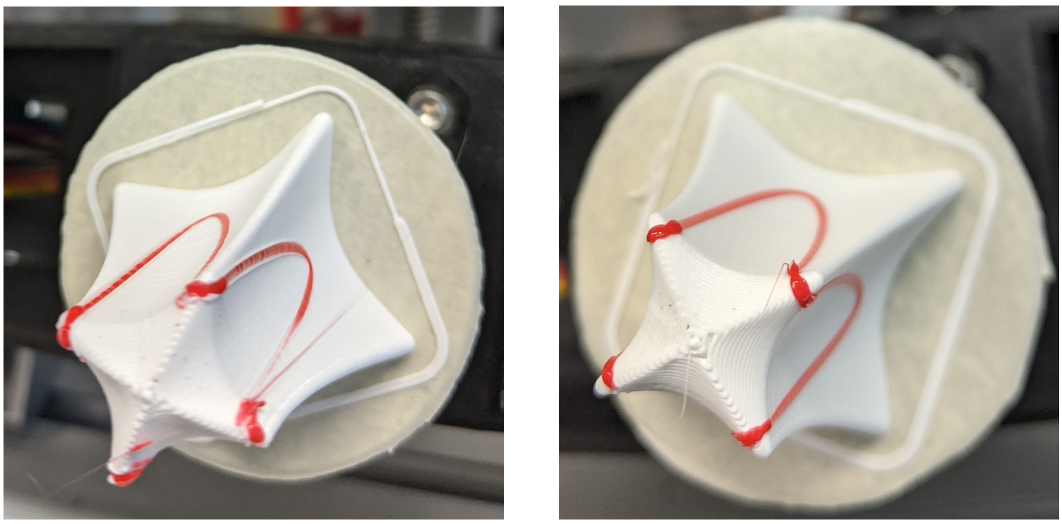

(a) (b)

Figure 6.20.: 5 axis combined print result using the 5 axis test object. (a) shows a result with the B axis initially calibrated and an idealistic model in the 5x slicer (b) shows the result using the full calibration results

- **Financial Constraint:** avoid expensive solutions

The points are addressed in order:

1. The human involvement in a standard calibration procedure after starting the printer now consist of homing the axes, removing the print bed, running the procedure and reattaching the print bed with a final homing of the rotary axes. The procedure still needs a small amount of human involvement, especially for transferring the results to the 5x slicer. Generally no human measurements are needed to get the system running. The full calibration for determining all the values is more labor-intensive, but also does not have to be performed often.

2. The main calibration of the printer is not very time-consuming and takes less than 10 minutes from startup to ready to print.

3. One objective of the project has been to use comparably low-cost solutions. The 3D probe costs less than 500€ and is the main part used for the measurements and one of the most expensive pieces of equipment on the printer. We consider our project to be low-cost, with a total cost of around 10,000€.

We consider the requirements set out at the start of the project to be fulfilled.

6.3.2. Internal Validation

The validation of the hardware components generally shows good results at the kinematic resolution of the printer. In general the internal, statistical validation of the data shows good results, facilitating the calibration of the printer. Though the A axis homing should be improved in the future.

6.3.3. External Validation

As the external validation is based on real world test prints, the interpretation is more subjective than for the quantitative results. Generally the external validation has been an important step to iteratively determine systematic errors of the measurements. The system has been able to show usable 5 axis print quality results in the real world using a simple calibration approach.

6.3.4. Project Goal Accomplishment

The positions of the axes have been measured to a satisfactory accuracy below $100\mu m$. The angles of the axes have been determined to a high confidence, though not better than $0.2°$. Real world tests showed sufficient results to accept the non-achievement of the goal. Consistent width extrusions have been achieved in most situations with only small imperfections in the integrated 5 axis tests.

7. Conclusion

7.1. Contributions

The main contributions of the thesis are the introduction of a calibration process for our or similar low-cost 5 axis printers, which requires limited human involvement. A central development are the tests for various elements of the calibration, which mostly isolate effects caused by a single component of each axis definition, while allowing for reasoning about the systematic errors remaining in the system. Further a suite of supporting GCode scripts and Jupyter notebooks have been developed to allow for the verification of the calibration and hardware used in the system. We showed that extensions beyond a line axis model should be considered for low-cost machines. Our results confirm the feasibility of 5 axis 3D printing using standard components.

7.2. Future Work

In the future multiple aspects could be improved upon and developed further.

Firstly the approaches explored before the current main measurement series could be refined to work well or even better in the future.

A potential way to improve the sphere based approach would be to use a smaller sphere on a levered calibration object (see figure 7.1). A steel ball bearing could then also be incorporated to ensure the shape of the sphere. Using an object not in the center of the rotation of the B axis should allow for measuring axis effects without having to expect a skewed axis. An approach mounting a sphere on the end of an arm could cause new problems, as the arm might flex. It might also apply too much force on the B axis motor, having it lose steps. The problem of using the 3D touch probe with spheres is also not addressed, though the exact known geometry of ball bearings could be used to characterize the probe.

A potential further development of the cross object approach was started but not carried over to real world tests. It was planned to reduce the number of points collected by the system, trading accuracy for speed. Further such points should be mostly collected using the X and Y direction probes, as the Z probes proved to be problematic in A rotated setting (See section 6.1.3). Such a process would also rely more on the given dimensions of the cross shape and less on measurement data. The fewer points would instead be used to fit two planes to the sides of the calibration cross. The Z orientation would then be the vector perpendicular to the two plane normals. From the two planes the normals (pointing away from the center) could then be reversed and both applied for the distance of half the cross arm size, giving a point on the center line of the cross. Using the probed height of the top of the cross, the plane through the center of the cross could be found, by translating it in the cross orientation by

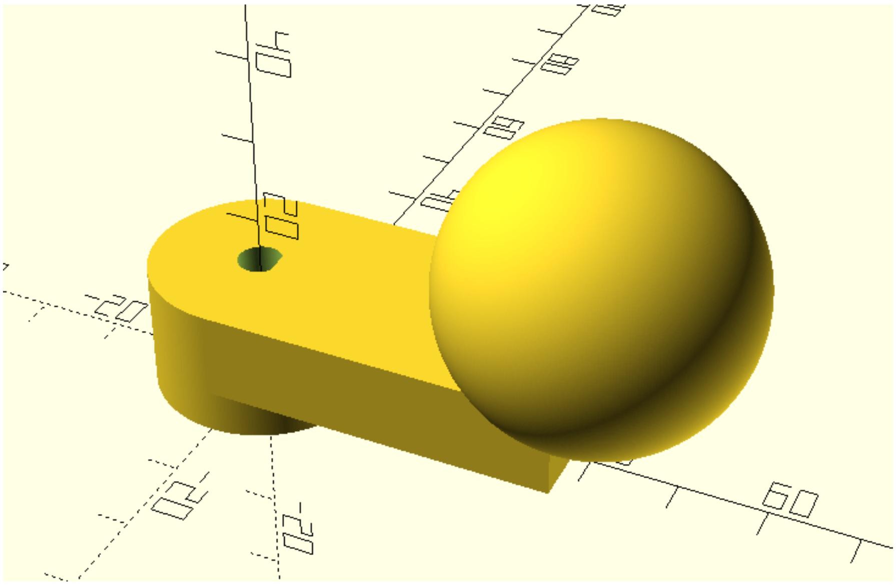

Figure 7.1.: Off-center calibration sphere for attachment onto the B Axis stepper motor

the arm length and half the cross arm size. By finding the intersection of the center plane and the center line the center point can be found.

Potentially a fitting approach for the whole cross shape could also be developed. The algorithm could find an appropriate set of center and orientation vectors matching a set of measured 3D points. Such an approach would allow for high flexibility in the measurement series performed on the cross.

The potential extensions would require a better calibration of the measurement probe itself, as systematic errors are not canceled out. Though this would need to be performed in any case of using a calibration object.

Regarding the general calibration of the machine multiple improvements could be explored as well.

The homing of the A axis could be improved, to result in a more level system. Potentially by measuring the encoder values more than once to correct for errors introduced in the movement. Further the PID system capability of the Duet3d printer could be used to create more reliable A and B axes movements. Though preliminary tests showed problems, especially with the A axis, as the load conditions change according to gravity.

The calibration process could be further optimized by only remeasuring the B axis position and keeping all other values. The full measurement would only need to be performed rarely. Optimally the process would work with the print bed installed.

In our lab other tools for the 3D printer have been developed, like the silver paste dispenser or the pick and place tool (see section 4.2.3 and 4.2.3). Using these tools, electronic components could be directly placed and connected in the printing process. The freedom of a 5 axis system would allow for such circuits placed in a 3D arrangement. The usage of these tools was not explored in this work and is one of the next avenues we would like to explore.

As the E3D toolchanger is a discontinued product, the transformation of the approach to other toolchanger platforms is needed for it to be useful in the future. Otherwise, a process for printers without a toolchanger could be explored, as Liu et al. have considered in their [9].

The real world analysis of the results is a quite manual and potentially error-prone process. Image processing using the integrated top down camera of the printer, especially for the B axis position test, could be used to find the systematic offset and correct it automatically.

The various tools are currently calibrated to each other using a software supported manual process. Using image processing the X/Y calibration of the tools to each other could be automated based on the bed camera. Although the calibration only needs adjustment after hardware changes.

A way to solve the computational restraints could be the use of Klipper[23], a system which incorporates a more powerful main controller, usually a Raspberry Pi [39], into the system. This further allows for the usage of standard data processing libraries which are available for Python as Klipper is based on the language. By extending the control system it would allow for the seamless integration of fitting algorithms and image processing workloads.

The possibility of using fitting algorithms for solving the axis calibration should be explored further as they could prove more effective than a separated, more simplistic process within the right circumstances.

In our project the slicer applies the correction of the axes as measured on the printer beforehand. The result usually only has to be adjusted when the hardware is changed. Another option would be compensation directly on the printer, by calculating the movements in object coordinates and then using inverse kinematics to correct the movements. Though this is computationally expensive for a 3D printer and the possibility of many edge cases emerging should be high, making this approach is rather development intensive. Klipper could also be used in this regard.

Further, in regard to the calibration the effect of temperature and other external factors on the axes could also be considered Potentially such effects are within the noise of our current system and would not be able to be determined with our hardware.

In general for the field of 5 axis 3D printing, open, free and performant slicers with 5 axis support are needed. As the hardware is reaching a state of usability in the low-cost 3D printing space, the availability of good software support is one of the key limiting features. The hardware enables practical development of such slicer without having to justify very expensive machines.

7.3. Closing

In this master thesis the topic of calibrating a 5 axis 3D printer was explored. We were able to successfully calibrate our custom, Open5x[34] based E3D toolchanger[38] to allow for printing directly onto objects. The process takes less than 10 minutes and only a small amount of human involvement. Although the results could be improved further, we were able to print using a standard $0.4mm$ nozzle without significant artifacts. Our approach is mostly limited by the machine, as the low-cost, mechanical setup introduced many challenges for the measurements. The available software for slicing for 5 axis printing is another limiting factor, with us resorting to using a slicer built in a sister project. The real world testing methodology developed in this thesis should allow others to calibrate their systems independent of the measurement method chosen. Though one of the key findings has been, that simple processes proved the most reliable while resulting in sufficient accuracy. We expect the prospect of 5 axis printing to become more important, especially in specialized scenarios like printing antennas or integrated electronics. Consequently, enabling research facilities to work with an affordable system should be a key factor in driving progress in the field.

Acknowledgement

I thank my supervisor Florens Wasserfall for the continued support throughout the thesis and the openness for motivating and fun discussions / testing sessions.

Special thanks go out to our lab technician German Junca, who designed most of the physical hardware of the printer and then brought it to live in the real world.

My thanks are extended to Daniel Ahlers for his help and thoughts regarding the elements of the thesis and the preceding laboratory work.

I express my thanks to the TAMS faculty of the University of Hamburg for enabling our research in the 3D printing laboratory.

Bibliography

Literature Resources

[1] Karlo Apro. *Secrets of 5-axis machining*. Industrial Press Inc., 2008, p. 15.

[2] Erik LJ Bohez. "Compensating for systematic errors in 5-axis NC machining". In: *Computer-Aided Design* 34.5 (2002), pp. 391–403.

[3] Guoxin Fang et al. "Reinforced FDM: Multi-axis filament alignment with controlled anisotropic strength". In: *ACM Transactions on Graphics (TOG)* 39.6 (2020), pp. 1–15.

[4] Freddie Hong et al. "5-axis multi-material 3D printing of curved electrical traces". In: *Additive Manufacturing* 70 (2023), p. 103546.

[5] Freddie Hong et al. "Open5x: Accessible 5-axis 3D printing and conformal slicing". In: *CHI Conference on Human Factors in Computing Systems Extended Abstracts*. 2022, pp. 1–6.

[6] Wenyuh Jywe, Tung-Hui Hsu, and C-H Liu. "Non-bar, an optical calibration system for five-axis CNC machine tools". In: *International Journal of Machine Tools and Manufacture* 59 (2012), pp. 16–23.

[7] WT Lei and YY Hsu. "Accuracy enhancement of five-axis CNC machines through real-time error compensation". In: *International journal of machine tools and manufacture* 43.9 (2003), pp. 871–877.

[8] WT Lei and YY Hsu. "Accuracy test of five-axis CNC machine tool with 3D probe–ball. Part I: design and modeling". In: *International Journal of Machine Tools and Manufacture* 42.10 (2002), pp. 1153–1162.

[9] Hao Liu, Lei Liu, and Kai Shen. "Rotary axis calculation for five-axis FDM printer using a point-fitting optimization method". In: *Applied Mathematics-A Journal of Chinese Universities* 37.2 (2022), pp. 258–271.

[10] Ren C Luo et al. "3D digital manufacturing via synchronous 5-Axes printing for strengthening printing parts". In: *IEEE Access* 8 (2020), pp. 126083–126091.

[11] Michalec Pawel, Laux Marius, Lisa Marie Faller, et al. "Supportless 5-Axis 3D-Printing and Conformal Slicing: A Simulation-based Approach". In: *2023 24th International Conference on Thermal, Mechanical and Multi-Physics Simulation and Experiments in Microelectronics and Microsystems (EuroSimE)*. IEEE. 2023, pp. 1–7.

[12] Jeevan Persad and Sean Rocke. "A survey of 3D printing technologies as applied to printed electronics". In: *IEEE Access* 10 (2022), pp. 27289–27319.

[13] B Ramos et al. “Optimal 3D printing of complex objects in a 5–axis printer”. In: *Optimization and Engineering* (2022), pp. 1–32.

[14] Yujie Shan et al. “Additive manufacturing of non-planar layers using isothermal surface slicing”. In: *Journal of Manufacturing Processes* 86 (2023), pp. 326–335.

[15] Hong Wei Tan et al. “3D printed electronics: Processes, materials and future trends”. In: *Progress in Materials Science* 127 (2022), p. 100945.

[16] Florens Wasserfall, Daniel Ahlers, and Norman Hendrich. “Optical in-situ verification of 3D-printed electronic circuits”. In: *2019 IEEE 15th International Conference on Automation Science and Engineering (CASE)*. IEEE. 2019, pp. 1302–1307.

[17] Xinyi Xiao and Sanjay Joshi. “Process planning for five-axis support free additive manufacturing”. In: *Additive Manufacturing* 36 (2020), p. 101569.

Technical Resources

[18] Bondtech AB. *LGX Lite eXtruder (with motor)*. `https://www.bondtech.se/product/lgx-lite-large-gears-extruder/`. Accessed: 2024-05-16. 2022.

[19] Robert McNeel & Associates. *Neu in Rhino 8*. `https://www.rhino3d.com/8/new/`. Accessed: 2024-04-03. 2024.

[20] Robert McNeel & Associates. *PrusaSlicer*. `https://github.com/prusa3d/PrusaSlicer`. Accessed: 2024-05-02. 2024.

[21] Boeeerb. *Introducing the LISIPAROI*. `https://www.lisiparoi.co.uk/index.htm`. Accessed: 2024-04-03. 2024.

[22] Klipper Contributors. *Bed leveling*. `https://www.klipper3d.org/Bed_Level.html#the-paper-test`. Accessed: 2024-04-03. 2021.

[23] Klipper3d Contributors. *klipper*. `https://github.com/Klipper3d/klipper`. Accessed: 2024-04-17. 2024.

[24] mjpg-streamer Contributors. *mjpg-streamer*. `https://github.com/jacksonliam/mjpg-streamer`. Accessed: 2024-05-03. 2021.

[25] Duet3D. *CAN connection basics*. `https://docs.duet3d.com/User_manual/Machine_configuration/CAN_connection`. Accessed: 2024-04-03. 2024.

[26] Duet3D. *Duet3D Magnetic Encoder*. `https://docs.duet3d.com/Duet3D_hardware/Accessories/Magnetic_Encoder`. Accessed: 2024-04-03. 2023.

[27] Duet3D. *GCode dictionary*. `https://docs.duet3d.com/User_manual/Reference/Gcodes`. Accessed: 2024-03-14. 2024.

[28] Duet3D. *GCode meta commands*. `https://docs.duet3d.com/User_manual/Reference/Gcode_meta_commands`. Accessed: 2024-03-14. 2024.

[29] Duet3D and Contributors. *RepRapFirmware*. `https://www.rhino3d.com/8/new/`. Accessed: 2024-04-03. 2024.

[30] E3D. *Research and Development: Motion System and Tool-Changer*. https://e3d-online.com/blogs/news/research-and-development-motion-system-and-tool-changer. Accessed: 2024-03-27. 2018.

[31] E3D. *Revo Belt Nozzles*. https://e3d-online.com/products/revo-belt-nozzles. Accessed: 2024-05-16. 2023.

[32] EdwardMakesThings. *E3D Tool Changer - Assembled*. https://www.thingiverse.com/thing:3880296. Accessed: 2024-03-14. 2019.

[33] Gina Häußge and Contributors. *OctoPrint*. https://octoprint.org/. Accessed: 2024-04-03. 2024.

[34] Freddie Hong et al. *Open5x*. https://github.com/FreddieHong19/Open5x. Accessed: 2024-01-02. 2022.

[35] Fortune Business Insights. *3D Printing Market Size, Share & COVID-19 Impact Analysis*. https://www.fortunebusinessinsights.com/industry-reports/3d-printing-market-101902. Accessed: 2023-11-13. 2023.

[36] Charles Jekel. *Least Squares Sphere Fit*. https://jekel.me/2015/Least-Squares-Sphere-Fit/. Accessed: 2024-04-03. 2015.

[37] CNC-STEP GmbH & Co. KG. *3D-Finder - Messtaster*. https://www.cnc-step.de/3d-finder-messtaster-taster/. Accessed: 2024-04-03. 2019.

[38] E3D-Online Ltd. *ToolChanger*. https://github.com/e3donline/ToolChanger. Accessed: 2024-01-02. 2019.

[39] Raspberry Pi Ltd. *Raspberry Pi 4*. https://www.raspberrypi.com/products/raspberry-pi-4-model-b/. Accessed: 2024-04-03. 2019.

[40] Raspberry Pi Ltd. *Raspberry Pi Documentation: Camera*. https://www.raspberrypi.com/documentation/accessories/camera.html. Accessed: 2024-04-03. 2024.

[41] Ilan E. Moyer. *core(X,Y) Principle of Operation*. https://corexy.com/theory.html. Accessed: 2024-04-03. 2012.

[42] Florens Wasserfall and Contributors. *OctoPNP*. https://github.com/platsch/OctoPNP. Accessed: 2024-04-03. 2024.

A. Appendix: Guide

This appendix is intended to serve as a guide to the usage of the 5 axis printer in the UHH laboratory.

Calibration Procedure

The calibration procedure is presented in two parts, with the first being the standard procedure normally performed. The extended procedure details the determination of the configuration parameters kept for multiple runs.

Standard Procedure

- **Homing of Axes:** The standard home all the printer is set up correctly and will home all the axes.
- **Calibration Procedure:** First remove the print bed and re-home the A and B axes. For the calibration procedure run the *Calibration AB* macro from the display or the web-overlay of the printer. The offset of the A axis from the B axis is printed to the console with the Z plane rotation of the A axis. Keep the results. The internal values are updated automatically. Reattach the print bed and re-home A and B.
- **Measurement of Print Bed Height:** To measure the print bed height pick up the 3D probe tool and run the *simple_z_probe.g* script with the position of $0, 0, 0$ and the Z probe 1. The Z height of the print bed is printed to the console.
- **Usage of the Results in the Slicer:** Within a standard slicer use the previously probed bed height as the Z offset to be able to print standard objects. In a 5 axis slicer, update the position and rotation of the A and B axes in the machine model. The printer expects the B axis position to be $0, 0, 0$. Adjust the height of base objects according to the probed height of the print bed.

Extended Procedure

The extended procedure expects the machine to be homed and if possible calibrated using the Standard Procedure.

- **A Axis Step:** The reference step for homing the A axis is determined by using the *a_get_reference_step.g* script. The step is printed to the console. Adjust the *target_step* variable in the *homea.g* script to set the value.

- **A Axis Scaling:** The scaling of the A axis can be wrong. This can be measured by probing the slope of the B axis' axle's flat side in the $\pm 90°$ positions of A. The slope should be close to 0 in both cases. If there is an imbalanced slope error, the scaling of the A axis has to be adjusted using the steps-per-degree(/mm) value in the firmware. Also adjust the value in the homing scripts. A symmetric error points to a 0 point error in the A Axis Step setting.

- **B Axis Step:** To get the reference step of the B axis chose a position and run *M569.5 P41.0 F"b-homing.csv" S1 A0 R0 D2 V0 H1* to collect the step value into the *b-homing.csv* file. Update the *target_step* value in *homeb.g*.

- **Tool Calibration:** For the calibration of the tools to each other in the X and Y position the OctoPNP plugin is used. In the settings of the plugin the bed camera is used to move the 3D touch probe tool to the bed camera's field of view. Use the interactive movements in the camera view to move the probe tool to the center. Finally, set the camera position and save. Next take all other tools and move them to the center of the camera. Save their tool offsets. For the Z component, the bed height is probed with the touch probe. The other tools are then calibrated using the paper method with manually adjusting the offsets in the *config-override.g* to give the same Z coordinate.

- **Probed Size Offset:** The probed size of an object is different to the actual size of the objects. To find the correction values for this, use a known size object. For example a printed cube and measure the size of it with calipers. Use the *probe_measure.g* script in the $\pm X$ and $\pm Y$ directions on the object to probe the sides of it. Then use the results in the *probe_test* notebook with the *comparision_to_hand_measured_sizes* procedure to find the offset in the X and Y directions of the object sizes. Set the Y correction value *Calibration AB* as the C parameter to *simple_a_measure.g* to use the result.

- **Z Axis Offset:** The Z position of the A axis can have a systematic offset. The offset can be found by rotating the A axis to $\pm 90°$ and doing a Z probe of the flat side of the B axle. Process the values in the *z_offset* notebook to the error of Z height. Add it to the *z_bias_correction* in the *update_g55.g* script.

- **B Axis Offset:** For the compensation of the systematic offset of the positional measurement of the B axis, print the B test line after having run the basic calibration of the printer. To generate the GCode for the test print, use the *generate_b_position_test_gcode* of the *axes_test* notebook. After printing the line, rotate B back to 0 and take a photo from the top of print bed. Use the *b_axis_compare* notebook to show the image and find error values interactively. Subtract the results from the *X_bias_correction* and *y_bias_correction* in the *update_g55.g* to apply the measured correction.

- **Z Rotation Offset:** The rotation in the Z plane resulting from the measurements was found to be off by a small margin. To correct for this, a *z_rotation_correction* variable has been added to the *update_g55.g* script. The correction factor can be found by using the A axis orientation test (see section 6.2.2). The orientation error can be measured by approximating the length of the line as 40 mm and measuring the start and end position using calipers. Calculating the slope on the surfaces gives an orientation error. The correction factor is used to rotate the orientation vector in the Z plane.

After finishing the procedure run the standard procedure again to start using the machine.

B. Appendix: Additional Scripts

Supporting software was developed to test ideas or work with the printer more easily. GCode scripts and Jupyter notebooks not directly relevant to the process described in the main part of the thesis are listed here.

GCode

A collection of helper/legacy GCode scripts were used. The are explained in the following paragraphs.

bed_probe.g: The *bed_probe* script is used to collect the height map data of the round print bed in a snaking pattern. It takes the X, Y and Z parameters as the center position of the bed to start at. The K parameter specifies the Z probe to use. Further the steps for the grid can be defined by the I parameter. The probe points are generated by iteratively filling a grid with points, which are then tested if they are within the circular print bed.

cross_measure.g: The measurements of the cross object as described in section 5.3. The X and Y parameters specify a coordinate of the approximate center of the cross as a starting point for the measurement of the cross. Using the A and B parameter rotations of the cross can be specified, limited to one axis. For A axis rotations of $\pm 90°$ and $0°$ are allowed. For B all $\pm 45°$ increments of $0°$. The result is written into the *global.cross_measurements* variable, separated into multiple lists for each phase of the measurement.

calibration_many_measure.g: To perform multiple measurements of the axes after each other the *calibration_many_measure.g* script can be used. The I parameter defines the iterations of measurements. The results are written to a file called *ab_values.out*.

a_get_reference_step.g: The reference step for the A axis has to be measured to use it in the Magnetic encoder based homing procedure (see section 5.1.2). The original Z probe on the E3D toolchanger is used to drive the A axis into it side way at both ends of the $\pm 90°$ rotations. The 0 position is set to the center of the probed rotation and the probed step value is printed to the console.

measure_pickup.g: The pick-up reliability is measured with the *measure_pickup* GCode procedure (see section 5.1.3). Using the X, Y and Z values a probing start position can be specified. The I parameter sets the count of repetitions for the pickup test. The results are printed to the console.

probe_measure.g: To characterize the probe according to the procedure described in section 5.1.5, *probe_measure* is used. The probe is moved from the current position in the direction vector specified by the X, Y and Z parameters in $10 \mu m$ steps for each component. The feedrate can be set with the F parameter. The movement is executed until the 3D probe is triggered and then backed up until the probe is not triggered anymore. This is repeated for I times. Results are written to the *probe_measure.out* file.

simple_z_probe.g: For probing the height of the print bed for specifying it in the standard slicer software the *simple_z_probe* script has been developed. The X, Y and Z parameter set a starting position for the bed probe, while K selects the Z probe to use. The script compensates for the tool length and gives the result in the currently used frame coordinates. Results are printed on the console.

sphere_measure.g: To the measure a sphere for the first approach discussed in section 5.2. The X and Y parameters specify the approximate center of the sphere. The rotation can be set using the A and B parameters. The top of the sphere is measured in a + shaped pattern with the default Z probe of the E3D printer.

Notebooks

Jupyter notebooks have been used to prototype ideas and process results.

ab_rot_axes: The *ab_rot_axes* notebook is used to combine the results of A and B axis measurements such that the closest approach is calculated. Further the rotation of the A axis in the Z plane is determined as the most relevant rotation deviation for our physical printer. The transformation from the B axis to the A axis is also given. At this point the functionality of the notebook has mostly been implemented on the printer in a GCode script replacing the notebook (See section 4.3.1).

bed_visualize: For visualizing the print bed as shown in the results section (See section 6.1.1) the *bed_visualize* notebook is used. It generates two 3D plots of the bed, one with all axes the same size and one with all axes fitted to the data. Secondly the two measured bed datasets are pre-filtered and fitted with planes and using those the tilt of the bed and the B axis are separated.

b_axis_compare: To check the positional offset of the B axis based on the B test print described in section 6.2.3 the *b_axis_compare* notebook was created. A photo of the result from the top has to be made and can then be displayed in the as the background of the plot generated by the notebook. The expected result of the test line based on an X and Y offset can then be simulated and overlaid on the image (see figure B.1). The offset can then be adjusted interactively, until the simulated line matches the real world measurement.

measurement_statistical_analysis: Results from the full repeated measurements (see section 5.4.1) are processed in the *measurement_statistical_analysis* notebook for statistical tests of the resulting 3D coordinates and orientations. Further the results are plotted in 3D or angle error space.

pickup_test: The *pickup_test* notebook is used to statistically analyzed the pick-up test results and visualizes the points in 3D space (see section 6.1.1).

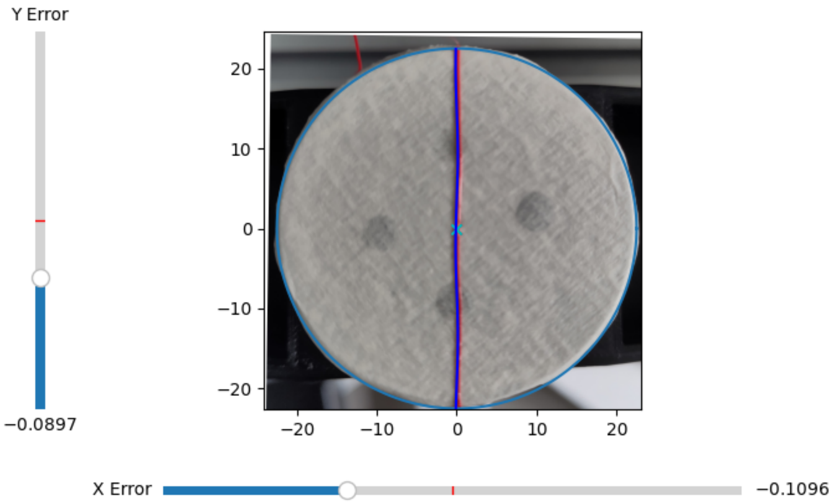

Figure B.1.: The B axis comparison interface

Eidesstattliche Erklärung

Hiermit versichere ich an Eides statt, dass ich die vorliegende Arbeit im Masterstudiengang Informatik selbstständig verfasst und keine anderen als die angegebenen Hilfsmittel — insbesondere keine im Quellenverzeichnis nicht benannten Internet-Quellen — benutzt habe. Alle Stellen, die wörtlich oder sinngemäß aus Veröffentlichungen entnommen wurden, sind als solche kenntlich gemacht. Ich versichere weiterhin, dass ich die Arbeit vorher nicht in einem anderen Prüfungsverfahren eingereicht habe.

Hamburg, den 1. Juni 2024

Tom Schmolzi

Veröffentlichung

Ich stimme der Einstellung der Arbeit in die Bibliothek des Fachbereichs Informatik zu.

Hamburg, den 1. Juni 2024

Tom Schmolzi